Two-point paraxial traveltime formula for inhomogeneous isotropic and anisotropic media: tests of accuracy

Umair bin Waheed [1], Ivan Pšenčík [2], Vlastislav Červený [3], Einar Iversen [4], and Tariq Alkhalifah [1]

[1]Physical Sciences and Engineering Division, KAUST, Saudi Arabia.
E-mail: umairbin.waheed@kaust.edu.sa, tariq.alkhalifah@kaust.edu.sa.
[2]Institute of Geophysics, Acad. Sci. of CR, Boční II, 141 31 Praha 4, Czech Republic.
E-mail: ip@ig.cas.cz.
[3]Charles University, Faculty of Mathematics and Physics, Department of Geophysics, Ke Karlovu 3, 121 16 Praha 2, Czech Republic. E-mail: vcerveny@seis.karlov.mff.cuni.cz.
[4]Norsar, P.O. Box 53, 2027 Kjeller, Norway. E-mail: Einar.Iversen@norsar.com.

SUMMARY

On several simple models of isotropic and anisotropic media we study the accuracy of the two-point paraxial traveltime formula designed for the approximate calculation of the traveltime between points S' and R' located in the vicinity of points S and R on a reference ray. The reference ray may be situated in a 3D inhomogeneous isotropic or anisotropic medium with or without smooth curved interfaces. The two-point paraxial traveltime formula has the form of the Taylor expansion of the two-point traveltime with respect to spatial Cartesian coordinates up to quadratic terms at points S and R on the reference ray. The constant term and the coefficients of the linear and quadratic terms are determined from quantities obtained from ray tracing and linear dynamic ray tracing along the reference ray. The use of linear dynamic ray tracing allows the evaluation of the quadratic terms in arbitrarily inhomogeneous media and, as shown by examples, it extends the region of accurate results around the reference ray between S and R (and even outside this interval) obtained with the linear terms only. Although the formula may be used for very general 3D models, in this paper we concentrate on simple 2D models of smoothly inhomogeneous isotropic and anisotropic ($\sim 8\%$ and $\sim 20\%$ anisotropy) media only. On tests, in which we estimate two-point traveltimes between a shifted source and a system of shifted receivers, we show that the formula may yield more accurate results than numerical solution of an eikonal-based differential equation. The tests also indicate that the accuracy of the formula depends primarily on the length and the curvature of the reference ray and only weakly depends on anisotropy. The greater is curvature of the reference ray, the narrower its vicinity, in which the formula yields accurate results.

Seismic Waves in Complex 3-D Structures, Report 23, Charles University, Faculty of Mathematics and Physics, Department of Geophysics, Praha 2013, pp. 149–184

1 INTRODUCTION

We study the accuracy of the two-point paraxial traveltime formula proposed by Červený et al. (2012). The formula can be used for the approximate determination of the two-point traveltime $T(R', S')$ between a point S' and another point R' arbitrarily chosen in the vicinities of two respective points S and R on a reference ray Ω (Figure 1). Ray Ω can be traced in a 3D laterally varying, isotropic or anisotropic model of elastic medium with or without structural interfaces. The two-point paraxial traveltime formula is based on the Taylor expansion of the two-point traveltime $T(R', S')$ with respect to the differences in spatial Cartesian coordinates $\mathbf{x}(S') - \mathbf{x}(S)$ and $\mathbf{x}(R') - \mathbf{x}(R)$ of points S' and S and points R' and R, with an accuracy up to quadratic terms. The constant term $T(R, S)$ in the expansion is known from tracing the reference ray. For the evaluation of the linear terms, slowness vectors $\mathbf{p}(S)$ and $\mathbf{p}(R)$, also known from the ray tracing of Ω, are necessary. For the evaluation of quadratic terms in the expansion, the tracing reference ray Ω is insufficient; dynamic ray tracing (DRT) or some other procedure providing quantities related to the second-order traveltime derivatives must also be performed. The dynamic ray tracing system used in this paper is a linear system of ordinary differential equations of the first order, which results from the differentiation of the ray tracing system with respect to ray parameters. As the system is linear, it is possible to construct its fundamental matrix $\mathbf{\Pi}(R, S)$. This matrix, specified as the identity matrix at point $R \equiv S$, is called here the *ray propagator matrix*. It plays a basic role in the paraxial ray methods. Once matrix $\mathbf{\Pi}(R, S)$ is known at point R of reference ray Ω, the solution of the DRT system at point R can be obtained by simple matrix multiplication for arbitrary initial conditions

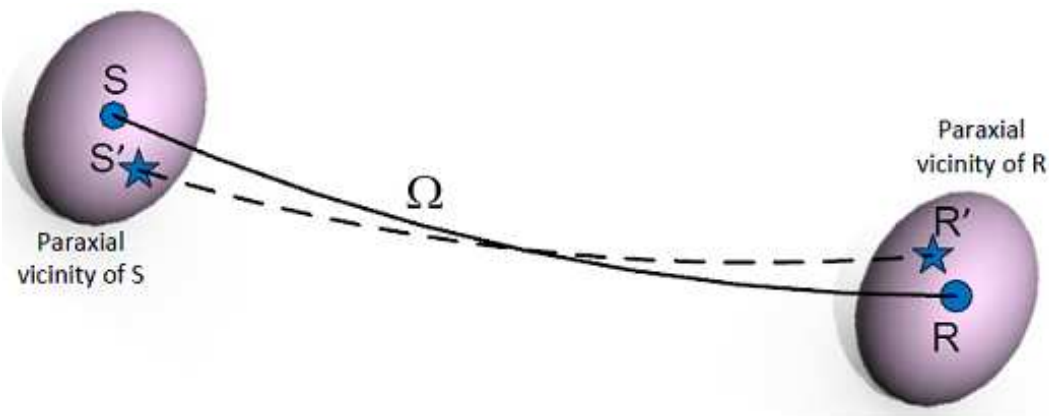

Figure 1: The traveltime between points S' and R' is estimated from the traveltime between points S and R on the reference ray Ω (black solid curve; dashed curve is shown only for illustration, no ray connecting S' and R' is necessary), along which the results of ray tracing and dynamic ray tracing in ray-centered coordinates are known.

at S. Note that, besides the linear DRT, also the nonlinear version of the DRT, based on the Riccati equation, has been used by some authors, see for example Gjøystdal et al. (1984). Here, however, we consistently use the linear DRT. When we refer to the DRT in the following text, we have the linear DRT in mind. For more details on ray tracing, linear and nonlinear dynamic ray tracing and ray propagator matrices see Červený (2001).

The DRT system and relevant ray propagator matrix can be computed along the reference ray in various coordinate systems (Cartesian, ray-centered, etc.). We use here a two-point paraxial traveltime formula with the DRT performed in ray-centered coordinates. Although DRT is performed in ray-centered coordinates, the positions of points S, R, S' and R' are specified in the Cartesian coordinate system. This makes the formula practical and flexible to use.

The quadratic traveltime approximation in the vicinity of the reference ray is usually called the *paraxial* traveltime approximation. The vicinity, in which the accuracy of the approximation is sufficient, is called the paraxial vicinity. The accuracy of the two-point paraxial traveltime formula depends on the results of the ray tracing and dynamic ray tracing along reference ray Ω. Both, in turn, depend on the first and second (DRT) spatial derivatives of the parameters of the medium at the points of Ω. Thus, as Vanelle and Gajewski (2002) put it, "the size of the (paraxial) vicinity depends on the scale of velocity variations in the model". Consequently, it is not easy to estimate quantitatively the accuracy of paraxial traveltimes and the size of the paraxial vicinity. The performed tests indicate significant dependence of the paraxial vicinity on the length of the reference ray. The longer the reference ray the greater size of the paraxial vicinity.

One possible way of estimating the accuracy of the two-point paraxial traveltime formula would be the use of the third-order terms of the Taylor expansion of the traveltime. This would, however, require knowledge of the third derivatives of the medium parameters, and that, in turn, would require models with continuous third derivatives of the model parameters. The majority of the presently used modeling techniques employs cubic splines, which do not guarantee continuity of the third derivatives. The use of splines of an order higher than cubic is feasible and is expected to yield better approximations to two-point paraxial traveltimes. On the other hand, such splines will lead to increased computation times, which thus represent a tradeoff between the accuracy and efficiency.

In this paper, we concentrate intentionally on simple 2D models without structural interfaces since they allow us to estimate easily the accuracy of the two-point paraxial traveltimes and to indicate the individual effects leading to the decrease of their accuracy. In more complicated models, it is more difficult to separate these effects (effects of inhomogeneity or anisotropy, effects of distance of points S and R, effects of distance of points S and S' and of points R and R', etc.).

The theory of two-point ray-theory traveltimes has a long history in wave sciences, mainly in optics. It was already studied by Hamilton (1837), who called the two-point traveltimes the point characteristics. Hamilton's theory of point characteristics (also known as characteristic functions) was recently extended by Klimeš (2009), see also Červený et al. (2012). Klimeš (2009) used the DRT in Cartesian coordinates and the corresponding 6×6 ray propagator matrix for the evaluation of two-point paraxial traveltimes $T(R', S')$. In this paper, we use the 4×4 ray propagator matrix in ray-centered coordinates. Hamilton's point characteristics also form the basis of the theory of opti-

cal systems, see, e.g., Luneburg (1964). Such systems were introduced to seismology by Bortfeld (1989), who established general surface-to-surface rules for rays and traveltimes of reflected and transmitted waves in media with structural interfaces. The applicability of Bortfeld's surface-to-surface method was considerably extended by Hubral et al. (1992) by using the DRT in ray-centered coordinates for layered inhomogeneous isotropic media. The method and its modifications have been used in various applications, see, e.g., Schleicher et al. (1993), Červený (2001), Červený and Moser (2007), Moser and Červený (2007). The accuracy of the method, however, has not been studied yet. In the surface-to-surface approaches, paraxial points S' and R' are situated on the surfaces passing through points S and R, respectively. This differs from the volume-to-volume approach used in this paper, in which paraxial points S' and R' can be situated arbitrarily in the 3D vicinities of points S and R. It is true that the two surfaces do not need to be physical, but once they have been chosen, the surface-to-surface method permits extrapolation in 4 coordinates only, while the volume-to-volume approach permits extrapolation in 6 coordinates. Moreover, our approach permits extrapolation also along the ray, while in the surface-to-surface method, the surface cannot be oriented so that the ray is tangent or nearly tangent to the surface.

Ursin (1982) proposed a traveltime formula closely related to the one used in this paper. He developed the Taylor type expansions for the travel time (parabolic formula) as well as its square (hyperbolic formula) around the reference source and receiver points. For the evaluation of the coefficients of the expansion, he used wavefront curvature matrices. Ursin (1982) showed that the hyperbolic form is exact for a homogeneous isotropic medium; see also Gjøystdal et al. (1984), Schleicher et al. (1993) and Appendix A of this paper. The hyperbolic formula of Ursin (1982) was used and generalized by many authors. Its accuracy as well as the accuracy of the parabolic formula were tested by Gjøystdal et al. (1984). More recently, the hyperbolic formula has been used to interpolate traveltimes (Vanelle and Gajewski, 2002) and for the determination of the geometrical spreading (Vanelle and Gajewski, 2003) in inhomogeneous isotropic or anisotropic media. The coefficients of the Taylor expansion were evaluated from traveltimes specified in known nodes of a coarse grid. The traveltimes were computed using an eikonal solver (not ray tracing and the DRT). Gjøystdal et al. (1984) made the first attempts to use the DRT in ray-centered coordinates for evaluating the coefficients of the Taylor expansion of squared traveltime in 3D laterally varying layered isotropic models. They, however, used a nonlinear form of DRT (Riccati equation), which did not allow construction of the ray propagator matrix. The ray propagator matrix was introduced in the context of two-point paraxial traveltimes by Červený et al. (1984), where the two-point paraxial traveltime formula for isotropic inhomogeneous media was presented for the first time. Mispel et al. (2003) studied the behavior of the parabolic and hyperbolic approximations in a typical seismic reflection imaging context, where the source and receiver points were fixed and the scattering point was allowed to vary.

In this paper, we use the parabolic formula of Červený et al. (2012). For computation in isotropic media, we use the standard ray tracer for computing reference rays with linear dynamic ray tracing along them. Along the reference rays, we compute standard ray-theory traveltimes. The ray-theory traveltimes obtained by ray tracing are used in the two-point paraxial formula and also for testing its accuracy. For computations in anisotropic media, we use first-order ray tracing and dynamic ray tracing (FORT and FODRT), see

Pšenčík and Farra (2005, 2007). This is a technique that allows for approximate, but relatively accurate, computations in inhomogeneous weakly and moderately anisotropic media. We test the accuracy of the two-point paraxial traveltime formula by comparing the traveltimes between S' and R' with the traveltimes obtained with the standard ray tracer in the isotropic case and with the FORT in the anisotropic case.

In the following section, we present the two-point paraxial traveltime formula derived by Červený et al. (2012) and briefly describe the quantities required to evaluate it. We then present numerical examples, which we use to illustrate the applicability of the formula in isotropic and anisotropic models. We also show its application to an experiment, in which we estimate the traveltimes between a shifted source and arbitrarily shifted systems of receivers. For this purpose, we use the traveltimes, ray-tracing and dynamic ray-tracing quantities obtained along the reference rays connecting the source and receivers before the shift. Results are shown for isotropic as well as anisotropic models. We end the paper with a short section containing concluding remarks. Appendix A is devoted to the analysis of the two-point paraxial traveltime formula in homogeneous media. Appendix B is devoted to the Shanks transform.

We use both the componental and matrix notation. In the componental notation, the upper-case indices $(I, J, K, ...)$ take the values 1 and 2, and the lower-case indices $(i, j, k, ...)$ the values 1,2, or 3. The Einstein summation convention is used. In the matrix notation, the matrices and vectors are denoted by bold upright symbols.

2 TWO-POINT PARAXIAL TRAVELTIME FORMULA

Let us consider a single reference ray Ω situated in a 3D laterally inhomogeneous, isotropic or anisotropic medium of arbitrary symmetry and two points, S and R, on it. Let us denote τ the traveltime variable along Ω, increasing from τ_0 at S to τ at R. The medium may or may not contain curved structural interfaces. Let us try to estimate the traveltime between points S' and R' arbitrarily chosen in the paraxial vicinities of points S and R, respectively. If traveltime $T(R, S)$ between S and R and the results of ray tracing and dynamic ray tracing along the reference ray are available, we can estimate $T(R', S')$ from the two-point paraxial traveltime formula proposed by Červený et al. (2012):

$$\begin{aligned} T(R', S') &= T(R, S) + \delta x_i^R p_i(R) - \delta x_i^S p_i(S) \\ &+ \tfrac{1}{2}\delta x_i^R [f_{Mi}^R (\mathbf{P}_2 \mathbf{Q}_2^{-1})_{MN} f_{Nj}^R + \Phi_{ij}(R)] \delta x_j^R \\ &+ \tfrac{1}{2}\delta x_i^S [f_{Mi}^S (\mathbf{Q}_2^{-1} \mathbf{Q}_1)_{MN} f_{Nj}^S - \Phi_{ij}(S)] \delta x_j^S \\ &- \delta x_i^S f_{Mi}^S (\mathbf{Q}_2^{-1})_{MN} f_{Nj}^R \delta x_j^R. \end{aligned} \tag{1}$$

The symbols $\mathbf{Q}_1 = \mathbf{Q}_1(R, S)$, $\mathbf{Q}_2 = \mathbf{Q}_2(R, S)$, and $\mathbf{P}_2 = \mathbf{P}_2(R, S)$ in equation 1 represent the 2×2 submatrices of the 4×4 ray propagator matrix $\mathbf{\Pi}(R, S)$ in ray-centered coordinates:

$$\mathbf{\Pi}(R, S) = \mathbf{\Pi}(\tau, \tau_0) = \begin{pmatrix} \mathbf{Q}_1(R, S) & \mathbf{Q}_2(R, S) \\ \mathbf{P}_1(R, S) & \mathbf{P}_2(R, S) \end{pmatrix} . \tag{2}$$

The ray propagator matrix $\mathbf{\Pi}(R,S)$ is determined by solving the DRT system

$$\mathrm{d}\mathbf{\Pi}(\tau,\tau_0)/\mathrm{d}\tau = \mathbf{S}(\tau)\mathbf{\Pi}(\tau,\tau_0) \tag{3}$$

along ray Ω from S to R, with initial conditions at $\tau = \tau_0$:

$$\mathbf{\Pi}(\tau_0,\tau_0) = \mathbf{I}\ . \tag{4}$$

Matrix $\mathbf{S}(\tau)$ in differential equation 3 is the 4×4 DRT system matrix, matrix $\mathbf{I}$ in equation 4 is the 4×4 identity matrix. For more details see Červený et al. (2012).

The other symbols in equation 1 are defined as follows:

$$\delta x_i^S = x_i(S') - x_i(S)\ , \qquad \delta x_i^R = x_i(R') - x_i(R) \tag{5}$$

and

$$\Phi_{ij} = p_i\eta_j + p_j\eta_i - p_ip_j\mathcal{U}_k\eta_k\ . \tag{6}$$

Symbols $x_i(S)$ and $x_i(R)$ denote the Cartesian coordinates of points S and R on reference ray Ω; $x_i(S')$ and $x_i(R')$ denote the Cartesian coordinates of points S' and R' situated in the paraxial vicinities of S and R, respectively, see Figure 1. Symbols p_i, $\mathcal{U}_i$ and η_i are the components of slowness vector $\mathbf{p}$, of ray-velocity vector $\boldsymbol{\mathcal{U}}$ and of the time derivative of $\mathbf{p}$ along the ray, $\boldsymbol{\eta}(\tau) = \mathrm{d}\mathbf{p}(\tau)/\mathrm{d}\tau$, respectively, all determined while tracing the reference ray. The upper indices S and R indicate that the corresponding quantities are considered at point S or R.

Symbols f_{Mi}^S and f_{Mi}^R $(M = 1,2)$ in formula 1 represent the Cartesian components of vectors $\mathbf{f}_1$ and $\mathbf{f}_2$ perpendicular to reference ray Ω at S and R, respectively. Vectors $\mathbf{f}_1$ and $\mathbf{f}_2$ are determined from equations:

$$\mathbf{f}_1 = \mathcal{C}^{-1}(\mathbf{e}_2\times\boldsymbol{\mathcal{U}})\ , \quad \mathbf{f}_2 = \mathcal{C}^{-1}(\boldsymbol{\mathcal{U}}\times\mathbf{e}_1)\ . \tag{7}$$

Here $\boldsymbol{\mathcal{U}}$ is the ray-velocity vector along reference ray Ω and $\mathcal{C}$ is the relevant phase velocity. Vectors $\mathbf{e}_I$ can be obtained by solving, along Ω, the vectorial, ordinary differential equation:

$$\mathrm{d}\mathbf{e}_I/\mathrm{d}\tau = -(\mathbf{e}_I\cdot\boldsymbol{\eta})\mathbf{p}/(\mathbf{p}\cdot\mathbf{p})\ . \tag{8}$$

Vectors $\mathbf{e}_I$ are situated in the plane tangent to the wavefront and form a right-handed orthonormal triplet with vector $\mathbf{e}_3 = \mathcal{C}\mathbf{p}$. It is sufficient to solve equation 8 for only one of the vectors $\mathbf{e}_1$, $\mathbf{e}_2$. The other can be determined from the condition of orthonormality of vectors $\mathbf{e}_i$. Note that vectors $\mathbf{f}_1$ and $\mathbf{f}_2$ need not necessarily be unit and orthogonal in anisotropic media.

Once reference ray Ω and the above-mentioned quantities calculated along it are available, the two-point paraxial traveltimes between points S' and R', arbitrarily chosen in the vicinities of S and R, can be calculated without a problem. Let us mention that formula 1 fails to work properly if the variation of the model parameters in the vicinity of the reference ray is too strong, or if matrix $\mathbf{Q}_2$ is singular at point R. The latter problem occurs when there is a caustic at point R or when point R is too close to S, see the tests later. This is physically understandable as we cannot extrapolate the traveltime to large distances from a short segment of the reference ray.

In the next section, in one example, we also test the formula for $T^2(R', S')$. It has the following form (Červený, Iversen, Pšenčík, 2012):

$$\begin{aligned} T^2(R', S') &= \Big(T(R, S) + \delta x_i^R p_i(R) - \delta x_i^S p_i(S)\Big)^2 \\ &+ T(R, S)\Big(\delta x_i^R [f_{Mi}^R (\mathbf{P}_2 \mathbf{Q}_2^{-1})_{MN} f_{Nj}^R + \Phi_{ij}(R)] \delta x_j^R \\ &+ \delta x_i^S [f_{Mi}^S (\mathbf{Q}_2^{-1} \mathbf{Q}_1)_{MN} f_{Nj}^S - \Phi_{ij}(S)] \delta x_j^S \\ &- 2\delta x_i^S [f_{Mi}^S (\mathbf{Q}_2^{-1})_{MN} f_{Nj}^R] \delta x_j^R\Big) \ . \end{aligned} \tag{9}$$

The meaning of the quantities appearing in formula 9 is the same as in formula 1. The formula for $T^2(R', S')$ was obtained by squaring formula 1 and neglecting the terms of higher order than two in $\delta\mathbf{x}$.

3 TESTS

We test the two-point paraxial traveltime formula 1 in models of homogeneous and inhomogeneous, isotropic and anisotropic media. Standard ray tracing and dynamic ray tracing along the reference ray from S to R are used in isotropic media, even in cases when analytic solutions are known. In anisotropic media, we use the first-order ray tracing (FORT) approach (Pšenčík and Farra, 2005, 2007) instead of standard ray tracing for anisotropic media, for which formula 1 was designed. Along first-order rays, we perform first-order dynamic ray tracing in ray-centered coordinates. Quantities obtained in this way are used in formula 1.

As an illustration of the accuracy of the two-point paraxial traveltime formula, we compare its results $T(R', S')$ with $T_{ex}(R', S')$, where $T_{ex}(R', S')$ is obtained from standard two-point ray tracing. We consider 2D models, mostly of vertically inhomogeneous media. Note that in 2D models of vertically inhomogeneous media, vectors $\mathbf{e}_I(\tau)$ and $\mathbf{f}_I(\tau)$ can be determined analytically, without solving equation 8.

We consider first the case of $S' \equiv S$ with the point source fixed at S. In this case, equations 1 and 9 simplify considerably since $\delta x_i^S = 0$, and several terms on the right-hand side of equations 1 and 9 vanish. Points R' are situated at the nodes of a rectangular grid covering the studied region. The separation of horizontal and vertical grid lines is 0.1 km. In addition to studying the complete formula 1 for the two-point paraxial traveltime, we also study the effects of the linear and quadratic terms in $\delta\mathbf{x}$ in formula 1. More precisely, we study formula 1 with the quadratic terms ignored, yielding the two-point traveltime $T_{lin}(R', S)$ (*lin* indicates that only linear terms are retained) and with the linear terms ignored, yielding the two-point traveltime $T_{quad}(R', S)$ (*quad* indicates that only quadratic terms are retained). This separation of "linear" and "quadratic" terms clearly shows, where they play an important role. The white curve (line) in the plots indicates the reference ray between point S and point R. If not specified otherwise, $S \equiv$ (0,0) and $R \equiv$ (2.5, 2.5).

3.1 Isotropic models

We first investigate the accuracy of formula 1 for $T(R', S)$ in a homogeneous isotropic medium. In certain situations in this case, it is possible to compare the approximate formulas with the exact, see Appendix A. Here we show the comparison of results of the approximate two-point paraxial traveltime formula and of the two-point traveltimes based on standard ray formulas. We emphasize again that we are studying the accuracy of the two-point paraxial traveltime formula 1 in all figures. Only in one figure, we briefly discuss the accuracy of $T^2(R', S)$. For supplementary test results in isotropic media, see Gjøystdal et al. (1984).

In Figure 2, we can see the traveltime differences $T(R', S) - T_{ex}(R', S)$ measured in seconds, where $T(R', S)$ stands for $T_{lin}(R', S)$ in the upper plot, for $T_{quad}(R', S)$ in the middle plot and for the complete two-point paraxial traveltime, given by formula 1, in the bottom plot. Note that $T(R, S) = 1.7678$ s. As shown in Appendix A, see equations A-2 and A-4, formula 1 for $T(R', S)$ reduces in a homogeneous medium to the formula for $T_{lin}(R', S)$ and yields the exact traveltime along the reference ray. This can be seen in the upper plot of Figure 2. Perpendicular to the ray, $T_{lin}(R', S)$ is constant, equal to the two-point traveltime $T(R, S)$ at point R on the reference ray. The exact traveltime is, therefore, always larger than $T_{lin}(R', S)$ in the vicinity of the reference ray. Thus, we can see only negative or zero (on the reference ray) traveltime differences in the upper plot. As the curvature of the wavefront (with the exact two-point traveltime on it) decreases with increasing distance from point S, the region of small traveltime differences (and thus the higher accuracy of $T_{lin}(R', S)$) broadens. In accordance with the conclusions of Appendix A, the accuracy of $T_{quad}(R', S)$ is very high along the normal to the reference ray at point R. The strong gradient of the traveltime differences parallel to the reference ray is caused by the linear term missing in $T_{quad}(R', S)$. It is interesting to see the combined effects of the linear and quadratic terms in the bottom plot of Figure 2. The bottom plot also shows that the two-point paraxial traveltime formula 1 increasingly underestimates the exact traveltime with increasing perpendicular distance from the reference ray between S and R. On the contrary, the approximate traveltimes are increasingly overestimated in the direction perpendicular to the reference ray beyond point R (this part of the reference ray is not shown). Figure 3 shows the same as the bottom plot of Figure 2, but in the form of isolines. It provides a better quantitative estimate of the accuracy of formula 1. The reference ray between S and R is shown as the bold black curve. We can see that the region of high accuracy of $T(R', S)$ forms a kind of cross at point R with the part perpendicular to the reference ray slightly curved.

In Figure 4, we can see the same as in Figure 2, but for the isotropic model with P-wave velocity of 2 km/s at $z = 0$ km and with a constant vertical gradient of 0.9 s^{-1}. $T(R, S) = 1.1594$ s in this case. We can see that the velocity gradient has distorted considerably the distribution of the traveltime differences as well as the trajectory of the reference ray. Note that the color scales for the differences of $T_{lin}(R', S)$, $T_{quad}(R', S)$ and $T(R', S)$ from $T_{ex}(R', S)$ are the same in Figures 2 and 4. In the upper plot of Figure 4, we can see that, except for the vicinity of point R, the reference ray is no longer a place of the highest accuracy of $T_{lin}(R', S)$. In fact, the region of the highest accuracy of $T_{lin}(R', S)$ around R splits both in the direction to and away from point S. The traveltime differences $T_{lin}(R', S) - T_{ex}(R', S)$ are no longer only negative or zero, they are now also

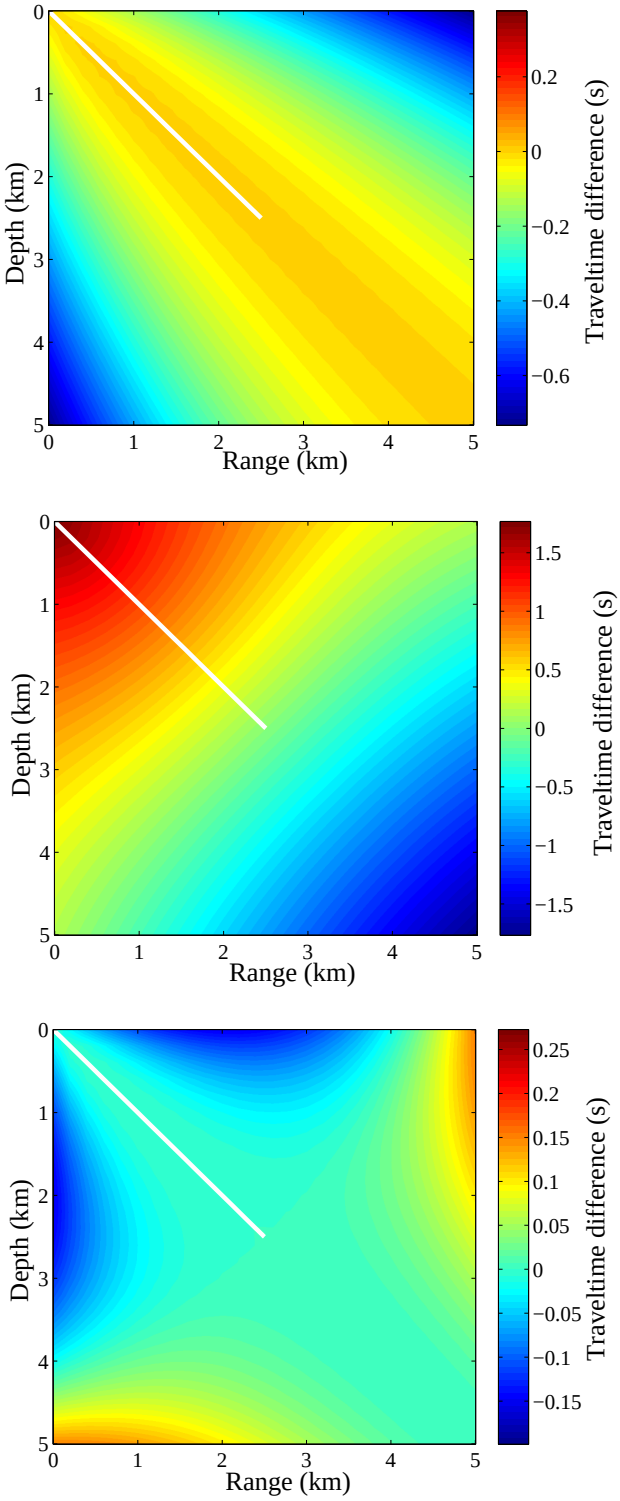

Figure 2: Traveltime differences $T(R', S) - T_{ex}(R', S)$ (in seconds) in the isotropic homogeneous model. $T_{ex}(R', S)$ - standard ray theory traveltime. Top: $T(R', S) = T_{lin}(R', S)$ - quadratic terms suppressed; middle: $T(R', S) = T_{quad}(R', S)$ - linear terms suppressed; bottom: $T(R', S)$ - the complete two-point paraxial traveltime determined from formula 1. Points S and R are situated at the beginning and end of the reference ray - white curve. Point S is situated at (0,0). Point R is situated at (2.5,2.5) and points R' in the grid covering the studied region.

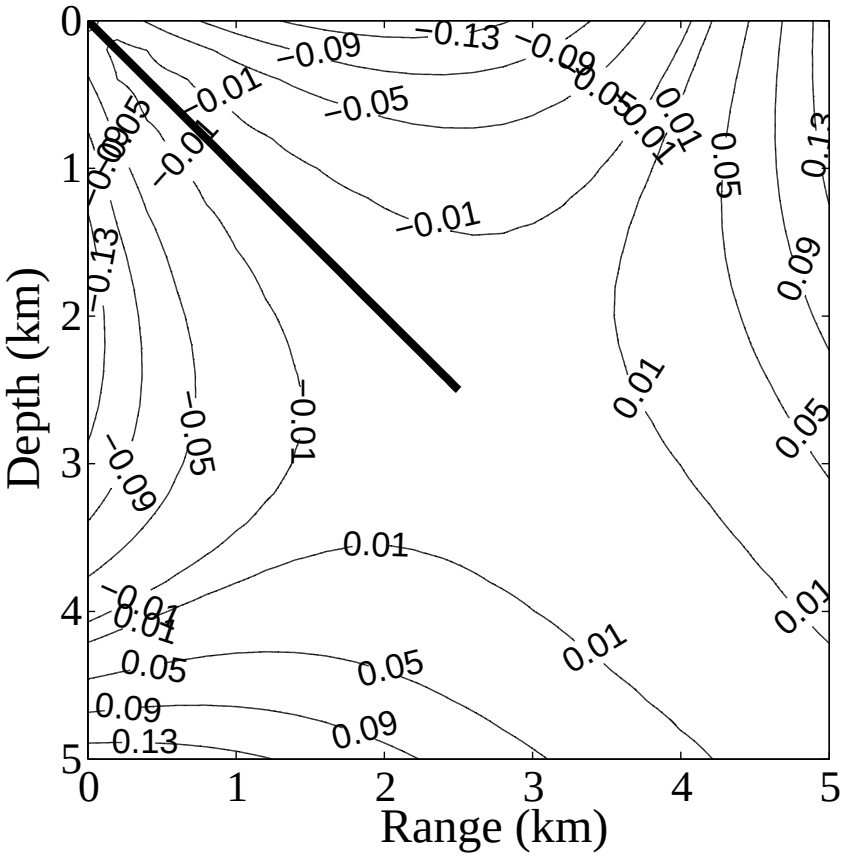

Figure 3: Traveltime differences $T(R', S) - T_{ex}(R', S)$ (in seconds) in the isotropic homogeneous model. $T_{ex}(R', S)$ - the standard ray theory traveltime. The plot corresponds to the bottom plot of Figure 2, where $T(R', S)$ is the complete two-point paraxial traveltime determined from formula 1. Points S and R are situated at the beginning and end of the reference ray - black curve. Point S is situated at (0,0). Point R is situated at (2.5,2.5) and points R' in the grid covering the studied region.

positive. Interesting is also behavior of $T_{quad}(R', S)$. The curve, along which $T_{quad}(R', S) = T_{ex}(R', S)$ is still perpendicular to the reference ray at R, but with increasing distance from it, it is strongly curved. The strong gradient of the traveltime differences $T_{quad}(R', S) - T_{ex}(R', S)$ along the reference ray remains. The map of the complete traveltime differences $T(R', S) - T_{ex}(R', S)$ in the bottom plot differs from its counterpart in Figure 2. The traveltime differences are not zero along the reference ray as they are in homogeneous media. The greatest distinction is a relatively large traveltime difference in the vicinity of point S. The symmetric picture from the bottom plot of Figure 2 is completely distorted due to the velocity gradient. This can also be seen in Figure 5, which shows the same as the bottom plot of Figure 4, but in the form of isolines.

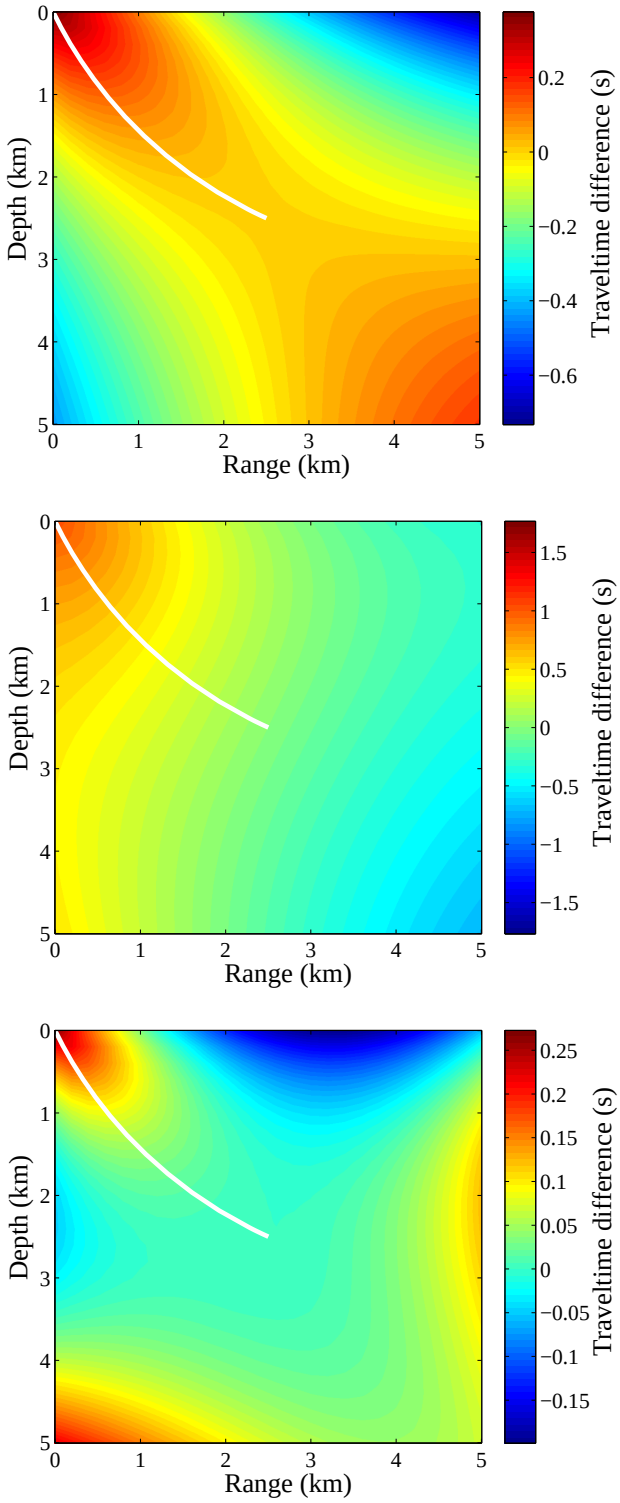

Figure 4: Traveltime differences $T(R', S) - T_{ex}(R', S)$ (in seconds) in the isotropic model with constant vertical gradient of 0.9 s^{-1}. $T_{ex}(R', S)$ - the standard ray theory traveltime. Top: $T(R', S) = T_{lin}(R', S)$ - quadratic terms suppressed; middle: $T(R', S) = T_{quad}(R', S)$ - linear terms suppressed; bottom: $T(R', S)$ - the complete two-point paraxial traveltime determined from formula 1. Points S and R are situated at the beginning and end of the reference ray - white curve. Point S is situated at (0,0). Point R is situated at (2.5,2.5) and points R' in the grid covering the studied region.

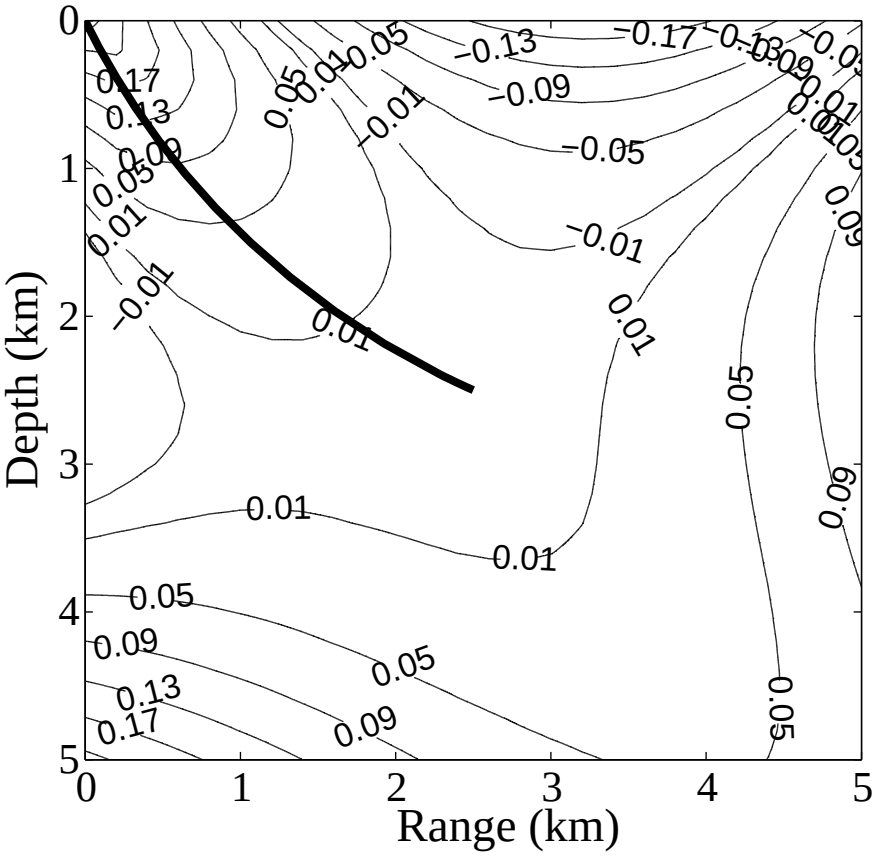

Figure 5: Traveltime differences $T(R', S) - T_{ex}(R', S)$ (in seconds) in the isotropic model with constant vertical gradient of 0.9 s^{-1}. $T_{ex}(R', S)$ - the standard ray theory traveltime. The plot corresponds to the bottom plot of Figure 4, where $T(R', S)$ is the complete two-point paraxial traveltime determined from formula 1. Points S and R are situated at the beginning and end of the reference ray - black curve. Point S is situated at (0,0). Point R is situated at (2.5,2.5) and points R' in the grid covering the studied region.

Next we study the effects of the length of the reference ray between the points S and R, specifically of the size of $T(R, S)$, on the accuracy and size of the region of applicability of formula 1. We consider an isotropic model with a P-wave velocity of 2 km/s at $z = 0$ km and a constant vertical gradient of 0.7 s^{-1} in all plots. Figure 6 shows the traveltime differences $T(R', S) - T_{ex}(R', S)$ for points R whose distance from point S is successively increasing. Point S is situated at (0,0), point R is situated successively at (0.1,0.1), (0.5,0.5), (1,1), (3,3), (4,4) and (5,5) and the corresponding two-point traveltimes $T(R, S)$ are 0.0695, 0.3225, 0.6041, 1.4221, 1.72 and 1.9717 s, respectively. Point S' is again chosen as coinciding with S, and points R' are situated at the grid points of a rectangular grid covering the studied region. For better comparison, we use the same color scale in all the plots. The reference ray is shown again as a white curve connecting points S and R.

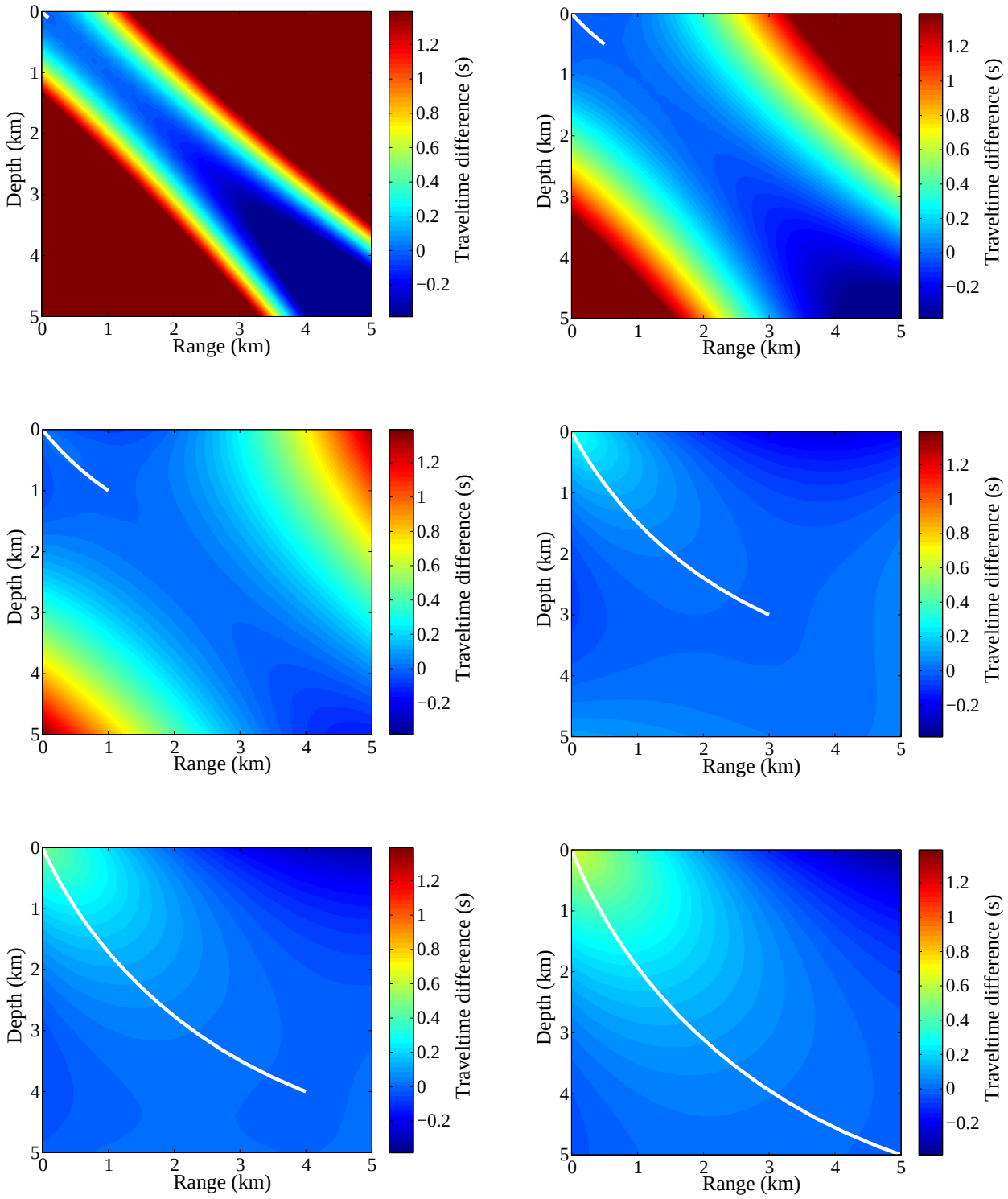

Figure 6: Traveltime differences $T(R', S) - T_{ex}(R', S)$ (in seconds) in the isotropic model with constant vertical gradient of 0.7 s^{-1}. $T(R', S)$ is the two-point paraxial traveltime determined from formula 1 and $T_{ex}(R', S)$ is the standard ray theory traveltime. Points S and R are situated at the beginning and end of the reference ray - white curve. Point S is situated at (0,0), point R at (0.1,0.1) - upper left, (0.5,0.5) - upper right, (1,1) - middle left, (3,3) - middle right, (4,4) - bottom left and (5,5) - bottom right. Points R' are situated in the grid covering the studied region.

In the upper left corner of Figure 6 we can see the confirmation of the theoretical observation that formula 1 is less accurate if the reference ray between S and R is very short (small $T(R,S)$). Point R is situated at (0.1,0.1) in this case. The region, in which formula 1 works relatively well, say with an accuracy well below 0.2 s, is very narrow. It underestimates the exact traveltimes in the direction of propagation (approximately along the diagonal of the plot). On the contrary, the traveltimes determined from formula 1 overestimate the exact traveltimes outside the narrow diagonal region. For R situated at (0.5,0.5) and (1,1), the region of accuracy under 0.2 s broadens and for R in the middle of the studied region, specifically at (3,3), the approximately determined traveltimes differ by less than 0.2 s from the exact ones in the whole studied region. With further increase of distance of R from S, for R situated at (4,4) and (5,5) the accuracy around S slightly decreases in the way observed in Figure 4, but remains high in the rest of the studied region.

In Figure 7, we compare the accuracy of equations 1 and 9. In the left column, we present the traveltime differences $|T(R',S) - T_{ex}(R',S)|$ calculated for $T(R',S)$ obtained from formula 1. In the right column, we present the traveltime differences for $T(R',S)$ obtained as the square root of $T^2(R',S)$ obtained from formula 9. The comparisons of the traveltime differences are made for the isotropic homogeneous model (top) and isotropic models with constant vertical gradients of 0.5 (middle) and 0.9 s^{-1} (bottom). Again the color scale is the same for all plots. As shown in Appendix A, equation 9 is exact in isotropic homogeneous media. This is clearly seen in the upper right plot of Figure 7. In inhomogeneous media, however, the accuracy of equation 9 rapidly decreases and becomes comparable or even lower than the accuracy of formula 1, see the right middle and bottom plots. Let us emphasize that all the above plots were obtained with the use of a *single reference ray* only.

To illustrate how formula 1 works in more complicated models, we test it in an isotropic anticline model, see the top plot of Figure 8, which shows the P-wave velocity distribution in the considered model. In this model, we perform a similar test as in Figures 2 and 4. The bottom plot of Figure 8 shows the traveltime differences $T(R',S) - T_{ex}(R',S)$ as in the bottom plots of Figures 2 and 4. Point S is situated outside the plot, at (-1,0); point R is located at (2.5,2.5). Both points are connected by the reference ray (white curve). Note that $T(R,S) = 1.733$ s. Despite the more complicated structure, the performance of formula 1 seems to be even better than in the 1D model of Figure 4 (note the different color scales). This indicates that the main factor reducing the accuracy of formula 1 is the curvature of the reference ray. The curvature of the reference ray in Figure 8 is smaller than in Figure 4.

So far, we have studied formula 1 with $S' \equiv S$, i.e., with S corresponding to a point source. In Figure 9, we test the performance of formula 1 for both points, S and R, shifted. Because in this experiment points S' and R' differ from points S and R, all terms on the right-hand side of formula 1 are involved in the procedure. The test is made in the isotropic model with a P-wave velocity of 2 km/s at $z = 0$ km and with a constant vertical gradient of 0.7 s^{-1}. Figure 9 shows the traveltime differences $T(R',S') - T_{ex}(R',S')$, where $T_{ex}(R',S')$ represents the standard ray-theory traveltime and $T(R',S')$ is the two-point paraxial traveltime obtained from formula 1 along the reference ray (denoted by the white curve) between S (outside the plot) and R. Point S situated at (0,- 0.5) in the upper plot and at (-0.5,0) in the bottom plot is shifted to point S' (0,0). Points R' are again

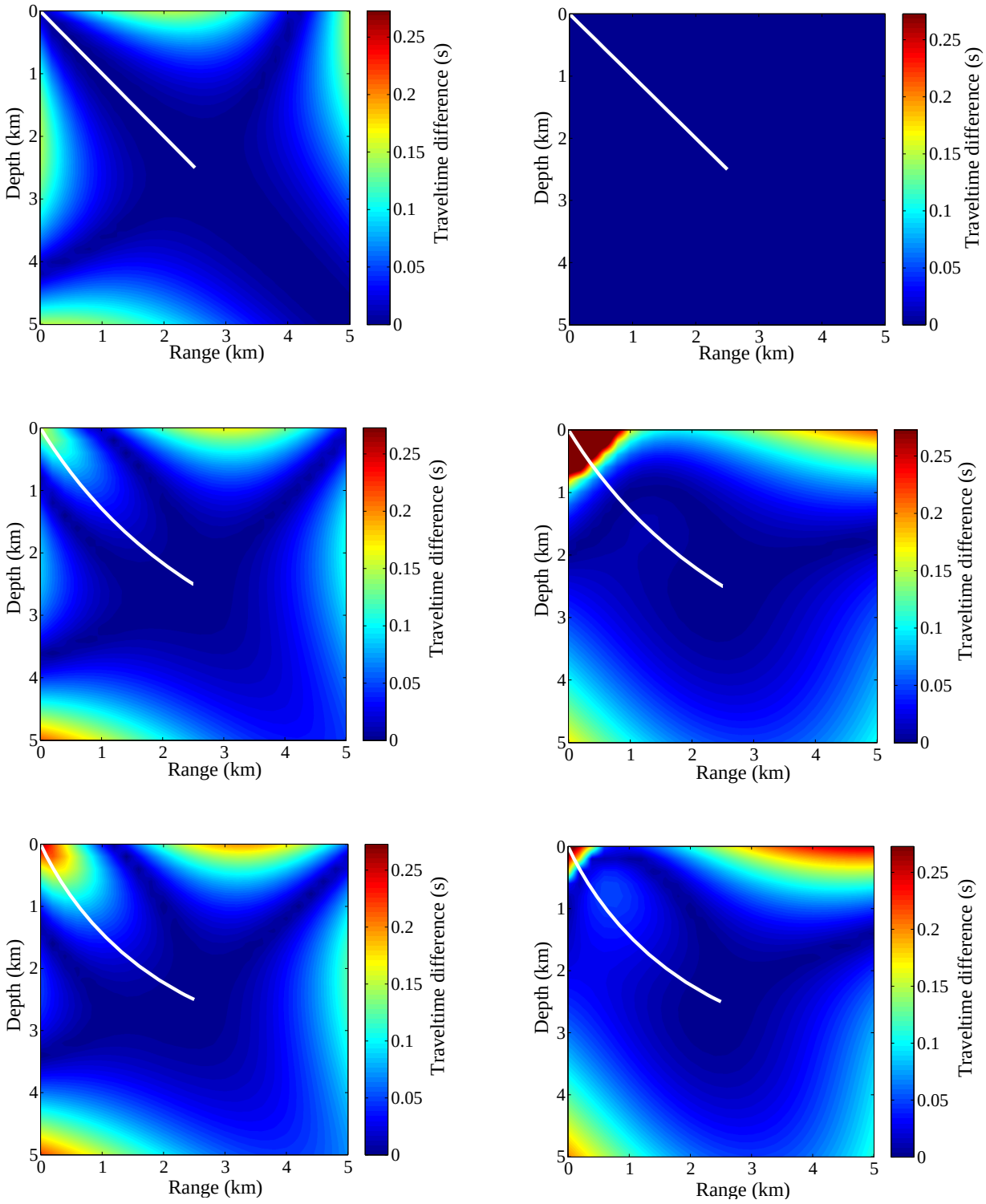

Figure 7: Traveltime differences $|T(R', S) - T_{ex}(R', S)|$ (in seconds) for $T(R', S)$ determined from formula 1 (left column) and for $T(R', S)$ determined as the square root of $T^2(R', S)$ calculated using formula 9. The isotropic homogeneous model (top), isotropic model with constant vertical gradient of 0.5 s^{-1} (middle) and 0.9 s^{-1} (bottom) are considered. $T_{ex}(R', S)$ - the standard ray theory traveltime. Points S and R are situated at the beginning and end of the reference ray - white curve. Point S is situated at (0,0), point R at (2.5,2.5) and points R' in the grid covering the studied region.

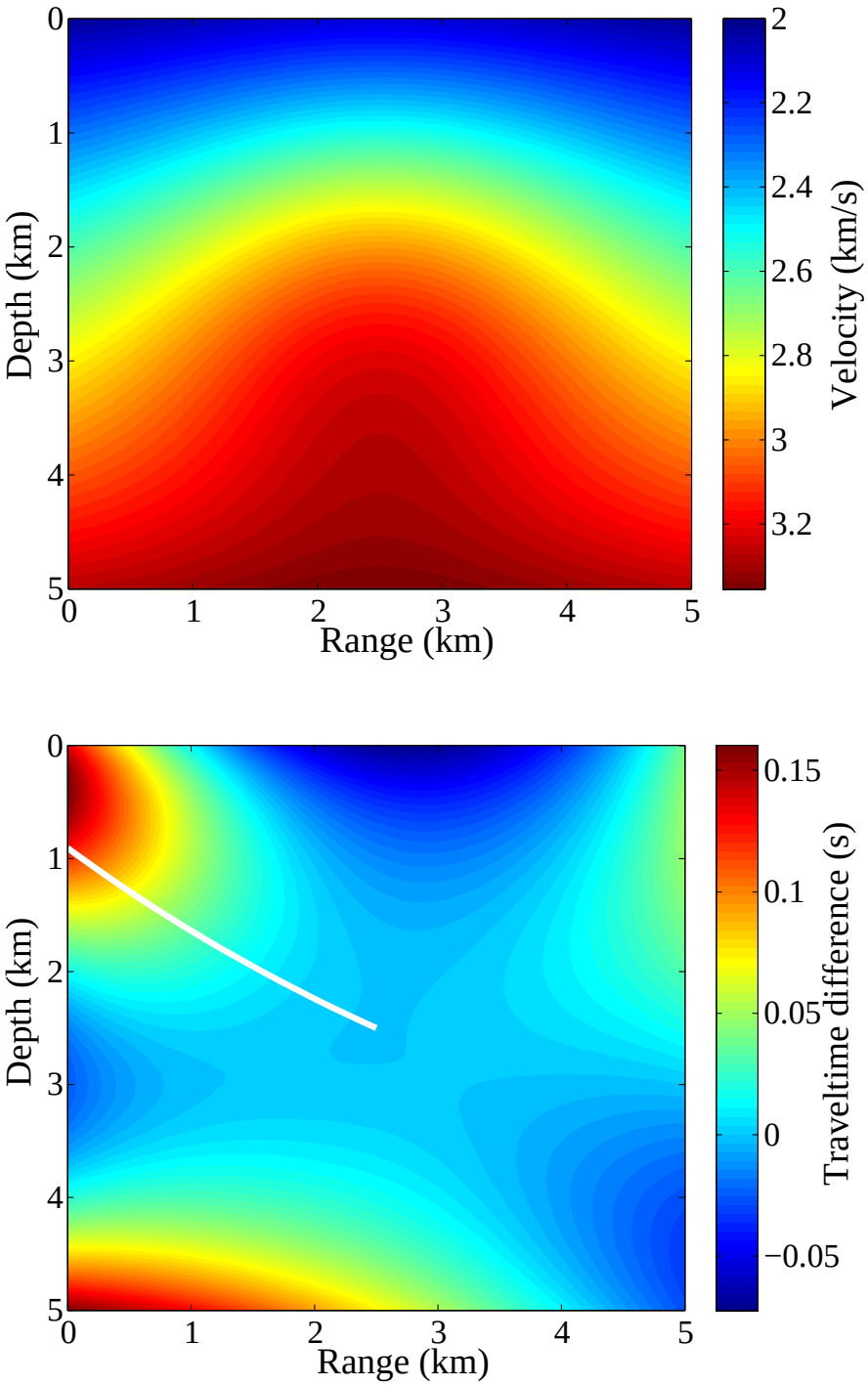

Figure 8: Isotropic anticline model (top) and traveltime differences $T(R', S) - T_{ex}(R', S)$ (in seconds) in this model (bottom). $T(R', S)$ is the two-point paraxial traveltime determined from formula 1 and $T_{ex}(R', S)$ is the standard ray theory traveltime. Points $S \equiv S'$ and R are situated at the beginning and end of the reference ray - white curve. Point S is situated at (-1,0) and, point R at (2.5,2.5). Points R' are situated in the grid covering the studied region.

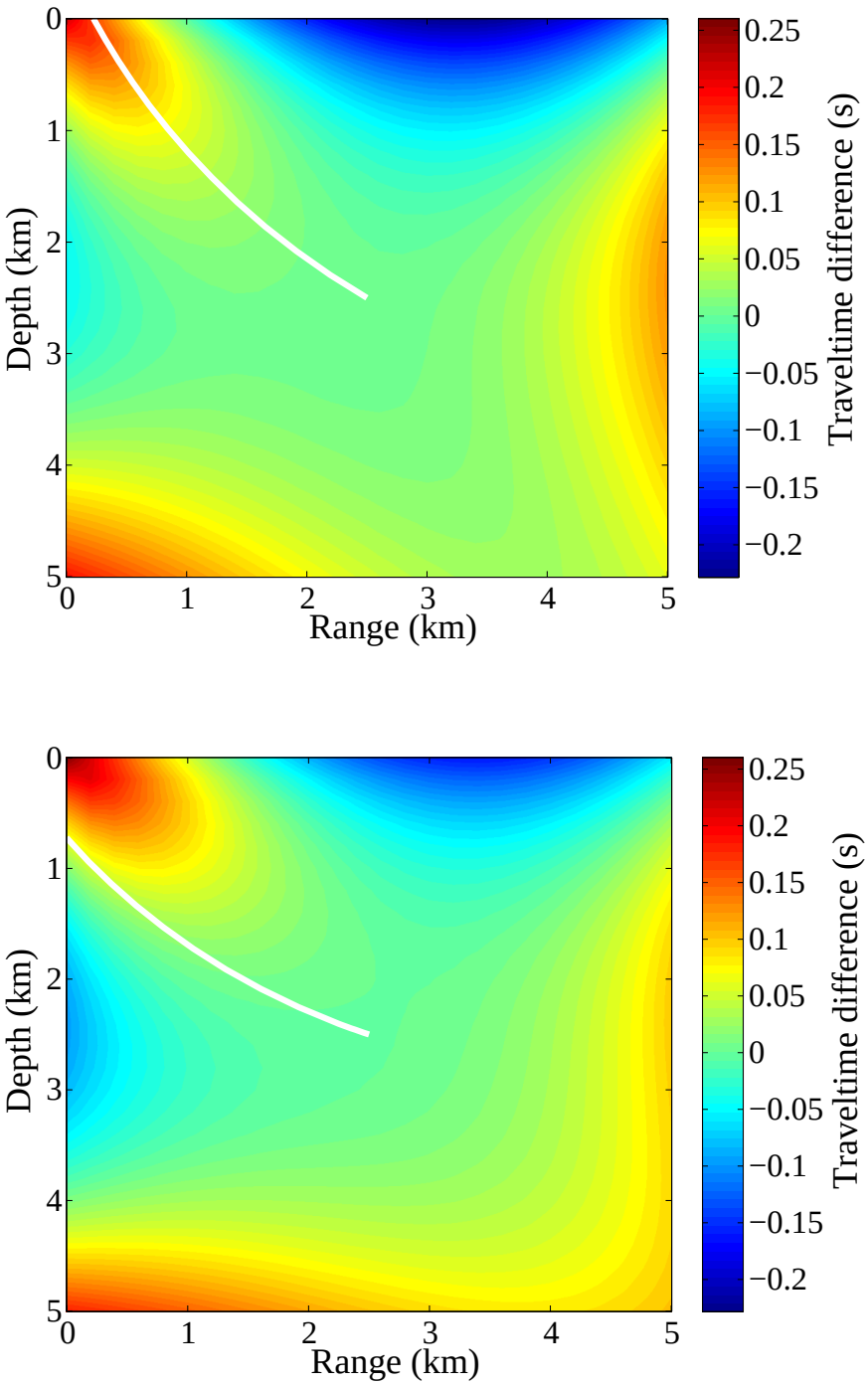

Figure 9: Traveltime differences $T(R', S') - T_{ex}(R', S')$ (in seconds) in the isotropic model with constant vertical gradient of 0.7 s^{-1}. $T(R', S')$ is the two-point paraxial traveltime determined from formula 1 and $T_{ex}(R', S')$ is the standard ray theory traveltime. Points S and R are situated at the beginning and end of the reference ray - white curve. Point S is situated at (0,-0.5) - top and at (-0.5,0) - bottom. Point R is situated at (2.5,2.5) in both plots. Point S' is in both plots at (0,0). Points R' are situated at the nodes of the grid covering the studied region.

situated at the nodes of a rectangular grid covering the model. Traveltimes $T(R, S)$ are 1.5 s in the upper plot and 1.3725 s in the bottom plot. We can see that the effects of the shift of point S are only small. When comparing the plots with the bottom plot of Figure 4 (where a higher gradient is used), effectively we can observe little change when S is shifted vertically (top). A slightly broader region of lower accuracy around point S' and a faster decrease of the accuracy away from point R can be observed for the horizontal shift of point S (bottom).

In the following, we use formula 1 in an experiment performed earlier by Alkhalifah and Fomel (2010), see the sketch in Figure 10. Alkhalifah and Fomel (2010) used two-point traveltimes calculated from one point source (S) to a system of receivers (R; in Figure 10 represented by two points R at selected nodes) distributed on a rectangular grid to estimate the traveltimes between the shifted source (S') and shifted receivers (R'). In Figure 10, source S is shifted horizontally by one grid interval and vertically by two grid intervals. The described procedure is important, for example, in Kirchhoff modeling, migration or in velocity estimation approaches. To calculate the two-point traveltimes, Alkhalifah and Fomel (2010) used the approach based on the numerical solution of the eikonal equation. Here we use the two-point paraxial traveltime formula 1. We can proceed in several ways. We can use a *single reference ray* between S and one of the points R situated in the middle of the grid and then use formula 1 to estimate $T(R', S')$. The results of such an experiment would not differ much from the tests in Figure 9.

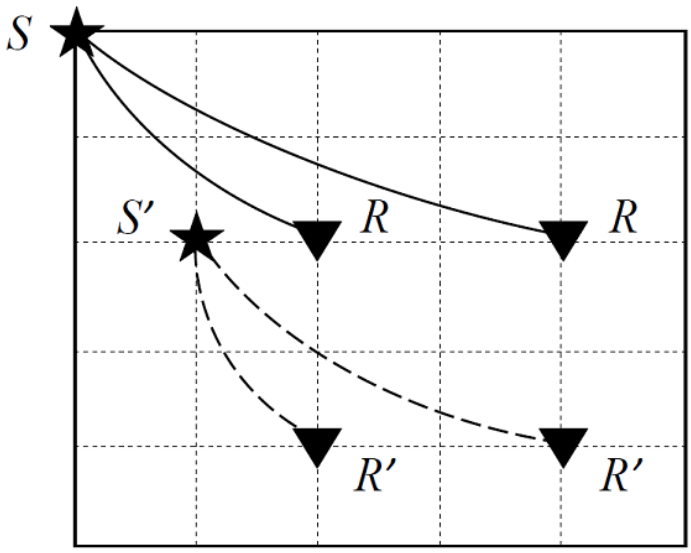

Figure 10: Use of the two-point paraxial traveltime formula to estimate two-point traveltime between shifted source S' and shifted receivers R'. Source S is shifted horizontally (by one grid interval) and vertically (by two grid intervals) to the new position S'. Every receiver R (the receivers are situated in all grid points; here represented by two selected grid points) is shifted vertically (by two grid intervals) to the new position R'. Two-point traveltimes along reference rays (black solid curve), from source S to receivers R are assumed to be known. Dashed curves are shown only for illustration, no rays connecting S' and R' are necessary).

To generate the plots in Figure 11, we have used a different and more accurate approach. We calculated the reference rays between source S and every receiver R, and solved the dynamic ray tracing equations along them. Using formula 1, we then recalculated the original two-point traveltime table $T(R, S)$ to yield a new table $T(R', S')$. The shifts of the source and of the receivers may be the same or different (in principle, each of the receivers R could be shifted in a different way). The original traveltime table $T(R, S)$ may be used to generate an arbitrary number of new tables $T(R', S')$ without need of new ray tracing and dynamic ray tracing.

The upper plot in Figure 11 shows the absolute values of the traveltime difference $|T(R', S') - T_{ex}(R', S')|$ in seconds, calculated by formula 1 for the model and configuration used by Alkhalifah and Fomel (2010). The model is isotropic with a P-wave velocity of 2 km/s at $z = 0$ km and a constant vertical gradient of 0.7 s^{-1}. Source S and all receivers R are shifted by 0.2 km in the positive z direction. In both plots of Figure 11, the shifted source S' is at (0,0) (the position of the original source S is thus outside the frames of the plots). Comparison with Figure 2b of Alkhalifah and Fomel (2010) shows that the traveltime differences of the two-point paraxial traveltime formula are: a) in most of the studied region by nearly one order lower (less than 0.001 s) than those of the eikonal-based approach, the highest traveltime differences (in the right upper corner) being around 0.003 s; b) varying negligibly in the whole studied region. The superiority of our approach is natural because Alkhalifah and Fomel (2010) used the first-order expansion while here, we have used the second-order expansion. The bottom plot in Figure 11 shows a map of the absolute traveltime differences corresponding to a vertical shift of the receivers different from the source. The source is shifted by 0.2 km and the receivers by 0.4 km. We can observe generally larger differences than in the upper plot. The largest differences are concentrated in the close vicinity of the shifted source S' (0,0). In a substantial part of the model, however, the traveltime differences do not exceed 0.005 s.

In the top plot of Figure 12 we show the traveltime differences $|T(R', S') - T_{ex}(R', S')|$ (in seconds) in the isotropic model with a constant vertical gradient of 0.7 s^{-1} and horizontal gradient of 0.5 s^{-1}. The source and receivers are shifted vertically by 0.8 km. The shifted source S' is located at (0,0). Despite the considerably large shift, the traveltime differences are reasonably small, not exceeding 0.025 s. For formulas like formula 1, which have the form of the Taylor expansion formula, Alkhalifah and Fomel (2010) suggest using the Shanks transform (Bender and Orszag, 1978). The Shanks transform can enhance the accuracy of such formulas if applied with care. The bottom plot of Figure 12 shows the top map after the application of the Shanks transform, see Appendix B. We can see that the accuracy has increased dramatically. The traveltime difference in the whole studied region does not exceed 0.005 s.

3.2 Anisotropic models

Previous tests were made on models of homogeneous or inhomogeneous isotropic media. Now we show several tests on anisotropic models. We start with the model of a transversely isotropic medium ($\sim$ 8% anisotropy) with the horizontal axis of symmetry (HTI) varying linearly with depth, see the schematic picture in Figure 13, which shows how the axis of symmetry varies with depth. We call the model the "twisted crystal model 8%".

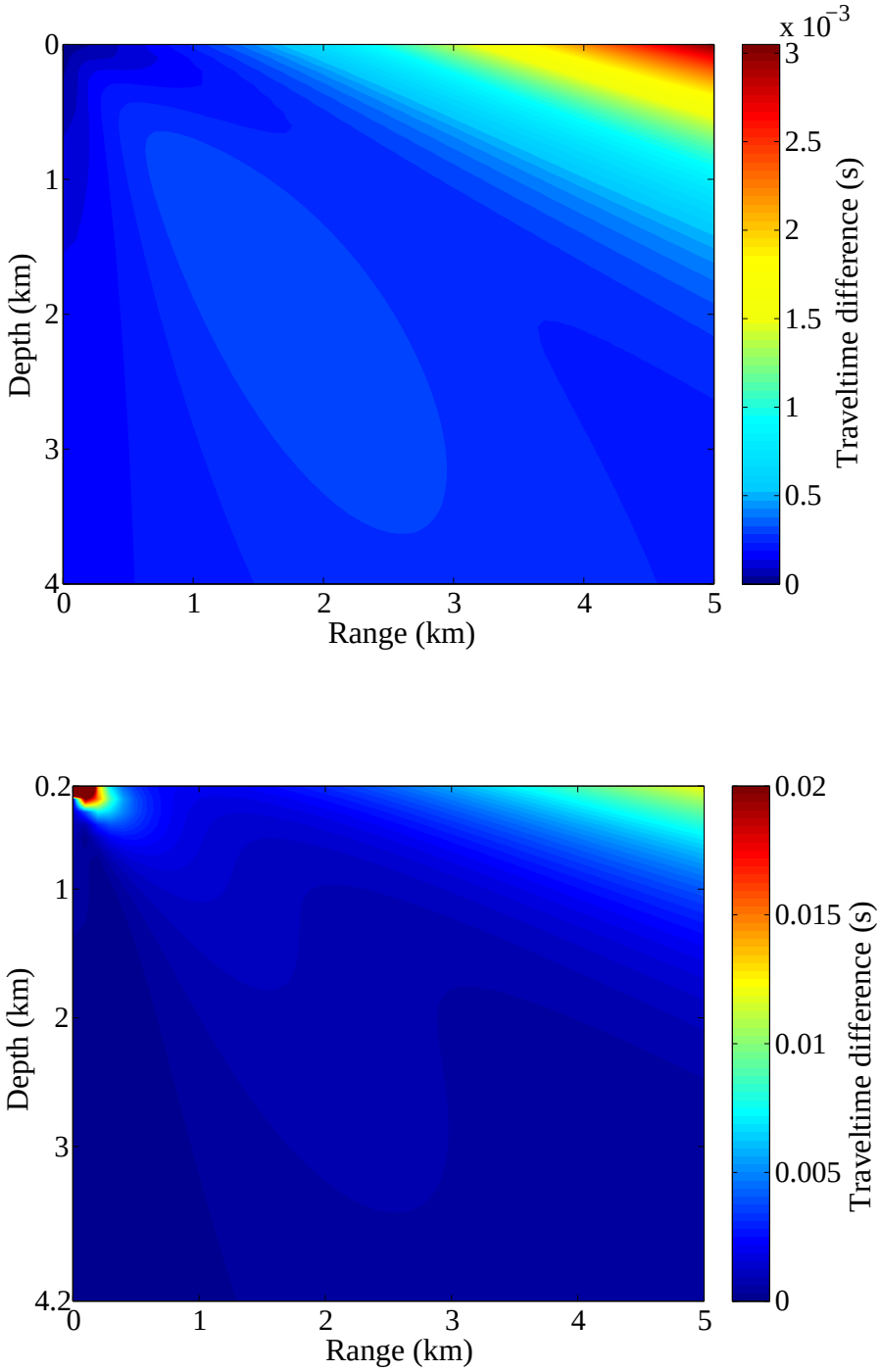

Figure 11: Application of the two-point paraxial traveltime formula to the estimation of the traveltimes between shifted source S' and the shifted system of receivers R'. The plots show the traveltime differences $|T(R', S') - T_{ex}(R', S')|$ (in seconds) in the isotropic model with constant vertical gradient of 0.7 s^{-1}. Shifted source S' at (0,0) and shifted receivers R' in the grid covering the studied region. Top: source S and receivers R shifted vertically by 0.2 km; cf. Figure 2b of Alkhalifah and Fomel (2010). Bottom: source S shifted vertically by 0.2 km, receivers R shifted vertically by 0.4 km.

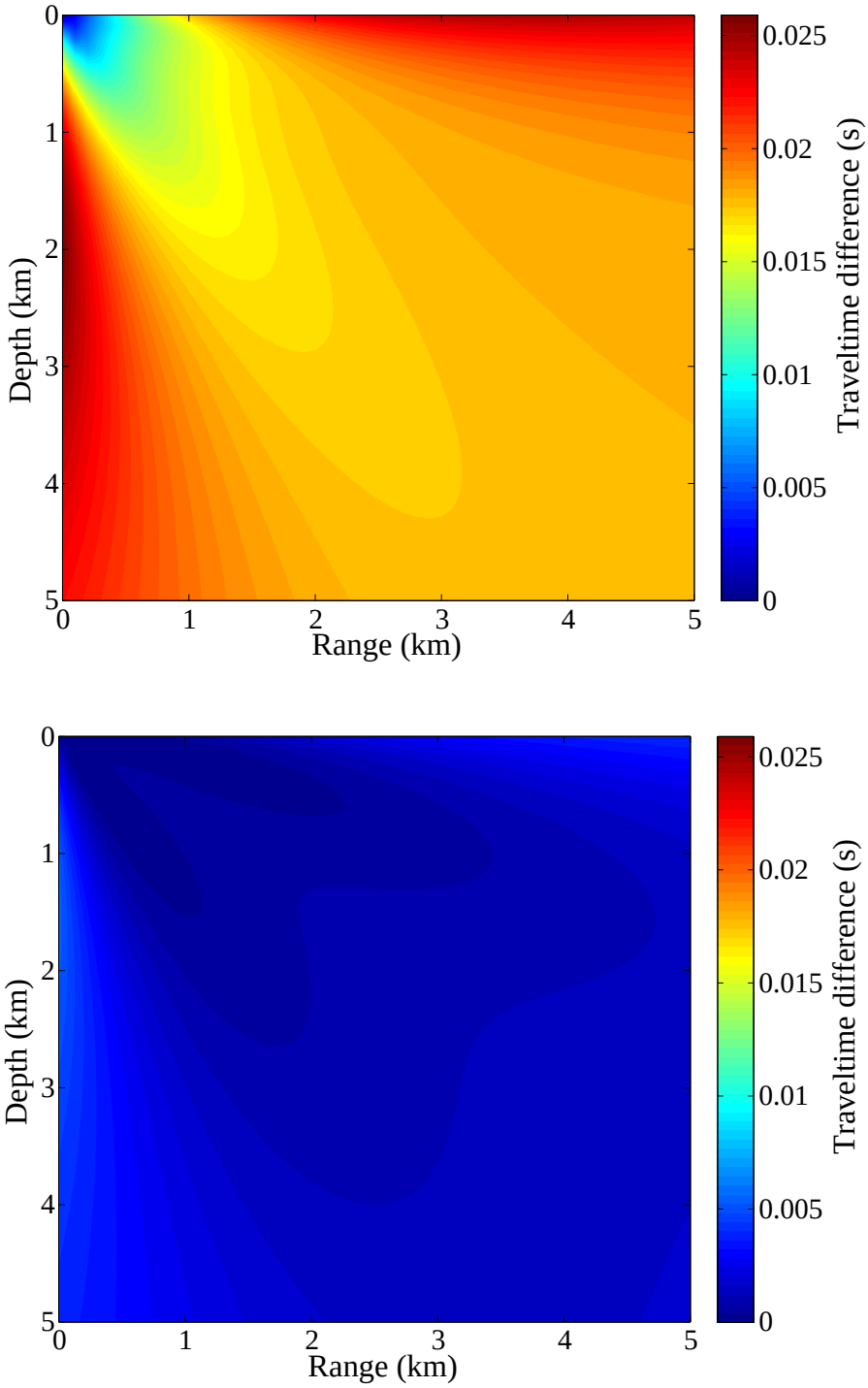

Figure 12: Application of the two-point paraxial traveltime formula to the estimation of the traveltimes between shifted source S' and the shifted system of receivers R'. The plots show traveltime differences $|T(R', S') - T_{ex}(R', S')|$ (in seconds) in the isotropic model with constant vertical gradient of 0.7 s^{-1} and horizontal gradient of 0.5 s^{-1}. Shifted source S' at (0,0) and shifted receivers R' in the grid covering the studied region. Top: the source and receivers shifted vertically by 0.8 km. Bottom: the same as above after the Shanks transform.

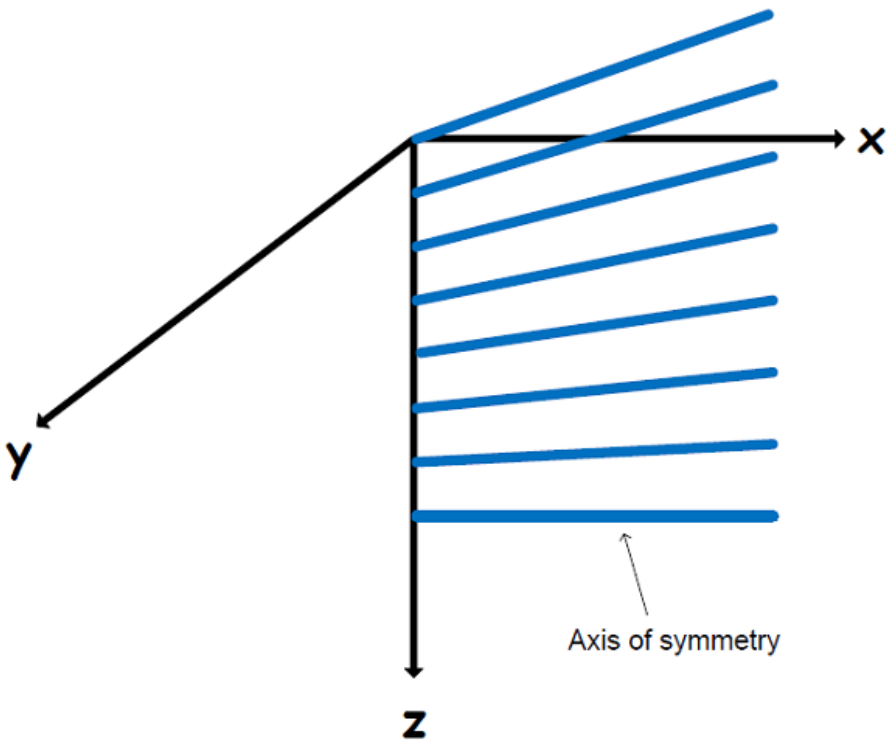

Figure 13: Schematic picture of rotating horizontal axis of symmetry in the "twisted crystal model 8%". The axis of symmetry makes an angle of -45° and 0° with the x-axis at $z = 0$ and $z = 5$ km, respectively.

We consider two realizations of the model. In one, which we call the "homogeneous model", density-normalized elastic moduli, measured in $(\mathrm{km/s})^2$, are constant throughout the model, only the axis of symmetry rotates with depth. In the other model, called the "inhomogeneous model", the density-normalized elastic moduli vary with depth in addition to the variation of the axis of symmetry. The moduli are specified as follows:

$$\begin{pmatrix} 14.485 & 4.525 & 4.755 & 0 & 0 & -0.58 \\ & 14.485 & 4.755 & 0 & 0 & -0.58 \\ & & 15.71 & 0 & 0 & -0.295 \\ & & & 5.155 & -0.175 & 0 \\ & & & & 5.155 & 0 \\ & & & & & 5.045 \end{pmatrix}$$

at $z = 0$ km and

$$\begin{pmatrix} 30.12750 & 10.0350 & 10.0350 & 0 & 0 & 0 \\ & 35.3475 & 11.3625 & 0 & 0 & 0 \\ & & 35.3475 & 0 & 0 & 0 \\ & & & 11.9925 & 0 & 0 \\ & & & & 11.2050 & 0 \\ & & & & & 11.2050 \end{pmatrix}$$

at $z = 5$ km. The Thomsen parameters (referenced to the axis of symmetry) are constant throughout: $\epsilon = 0.0866$ and $\delta = 0.0816$. In the "homogeneous model" the matrix for $z = 0$ km is used throughout the model, in the "inhomogeneous model" the density-normalized elastic moduli between $z = 0$ and 5 km are obtained by linear interpolation from the above values. In both cases, the axis of symmetry makes an angle of -45° with the x-axis at $z = 0$ km and 0° at $z = 5$ km. We consider $S' \equiv S$ at (0,0) and point R at (2.5,2.5). This again leads to considerable simplification of equation 1 since $\delta x_i^S = 0$, and several terms on the right-hand side of equation 1 vanish.

In Figure 14, we can see that the behavior of the traveltime differences $T(R', S) - T_{ex}(R', S)$ in the homogeneous "twisted crystal model 8%" resembles very much their behavior in the homogeneous isotropic model, see Figure 2. $T(R, S) = 0.917$ s in this case. The greatest difference between Figures 2 and 11 are the traveltime differences. For $T_{lin}(R', S)$ and $T_{quad}(R', S)$, the differences in Figure 14 are about half of the differences in Figure 2. The differences of the complete two-point paraxial traveltime are even smaller. The explanation is simple. The average velocity in the homogeneous twisted crystal model is approximately 4 km/s, while in the homogeneous isotropic model it is 2 km/s. Due to this, $T(R, S)$ in Figure 2 is 1.7678 s and in Figure 14, it is 0.917 s. For higher velocities, the traveltime differences are smaller. Figure 15 shows, as in the isotropic case, the same as the bottom plot in Figure 14, but in the form of isolines. We can see that the region of high accuracy of $T(R', S)$ again forms a kind of cross at point R, similarly as in isotropic media.

Figure 16 shows the same as Figure 14, but for the inhomogeneous "twisted crystal model 8%". In this case, $T(R, S) = 0.8069$ s. The resemblance to Figure 4 is not as strong as in the case of the homogeneous models. This is mostly caused by the different gradients in Figures 4 and 16. The fact that the gradient used to generate Figure 16 is weaker is indicated by the small curvature of the reference ray connecting points S and R. Since the average velocity in the model used to generate Figure 16 is approximately 5 km/s, the differences of the two-point paraxial traveltime $T(R', S)$ in Figure 16 are again substantially smaller than in Figure 4. The bottom plot of Figure 16 in the form of isolines can be seen in Figure 17.

Figure 18 shows the traveltime differences $|T(R', S) - T_{ex}(R', S)|$ in seconds for a similar experiment as in Figure 12, now for the inhomogeneous "twisted crystal model 8%". The source and receivers are shifted vertically by 0.8 km. The shifted source S' is located at (0,0). Despite the considerably large shift, the traveltime differences shown in the upper plot are small, not exceeding 0.005 s. In a large part of the studied region, they do not exceed 0.003 s. The bottom plot shows, as in Figure 12, the traveltime differences after application of the Shanks transform. As in the isotropic case, we can see a dramatic reduction in the traveltime differences. They do not exceed 0.002 s in the whole region;

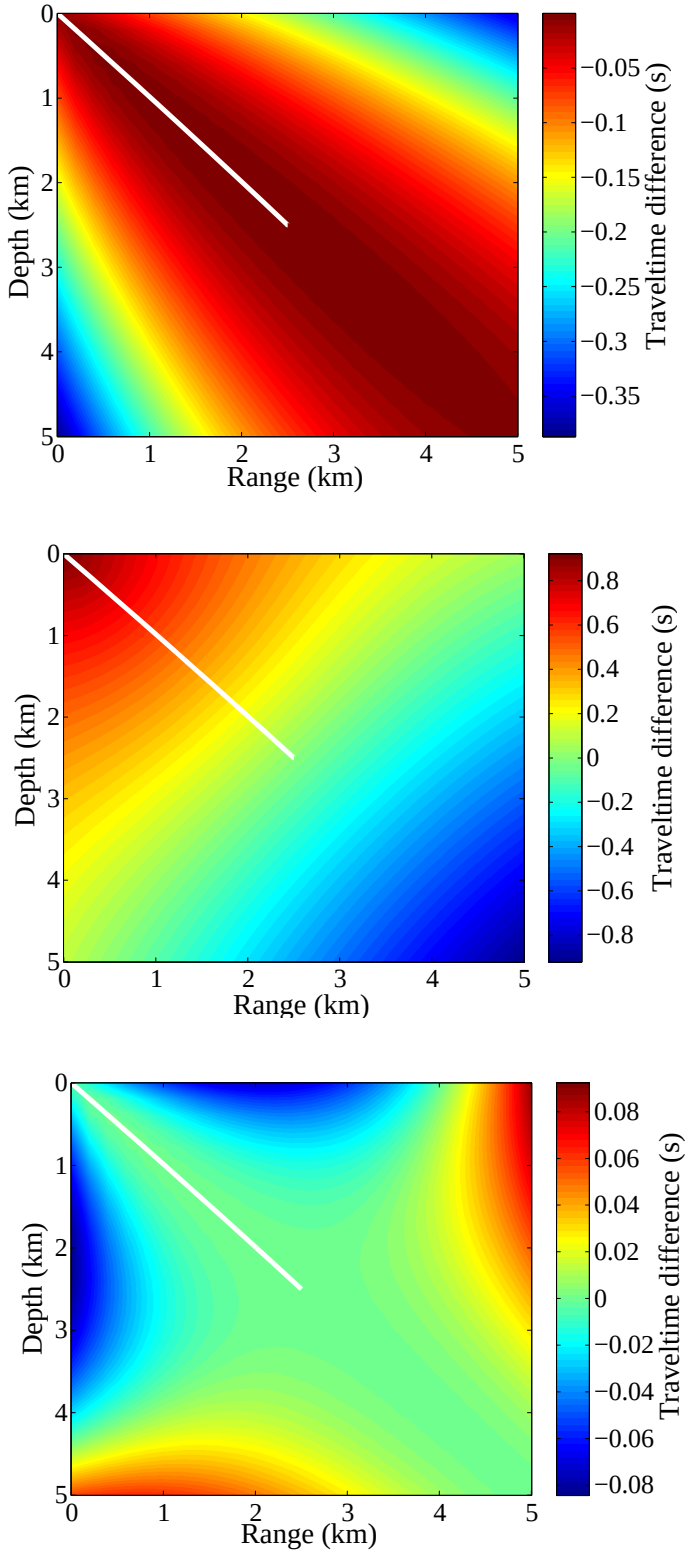

Figure 14: Traveltime differences $T(R', S) - T_{ex}(R', S)$ (in seconds) in the homogeneous "twisted crystal model 8%". $T_{ex}(R', S)$ - FORT traveltime. Top: $T(R', S) = T_{lin}(R', S)$ - quadratic terms suppressed; middle: $T(R', S) = T_{quad}(R', S)$ - linear terms suppressed; bottom: $T(R', S)$ - the complete two-point paraxial traveltime determined from formula 1. Points S and R are situated at the beginning and end of the reference ray - white curve. Point S is situated at (0,0). Point R is situated at (2.5,2.5) and points R' in the grid covering the studied region.

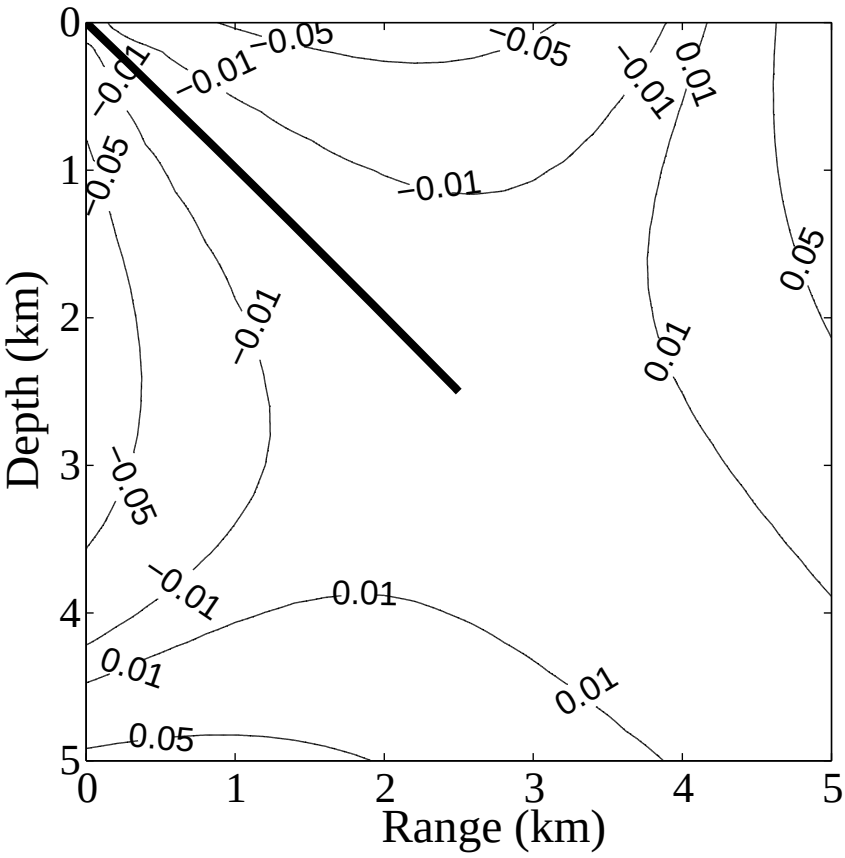

Figure 15: Traveltime differences $T(R', S) - T_{ex}(R', S)$ (in seconds) in the homogeneous "twisted crystal model 8%". $T_{ex}(R', S)$ - FORT traveltime. The plot corresponds to the bottom plot of Figure 14, where $T(R', S)$ is the complete two-point paraxial traveltime determined from formula 1. Points S and R are situated at the beginning and end of the reference ray - black curve. Point S is situated at (0,0). Point R is situated at (2.5,2.5) and points R' in the grid covering the studied region.

mostly they are even smaller. In contrast to the upper plot, the traveltime differences vary only negligibly.

Figure 19 shows the same as Figure 18, but for the model with the stronger anisotropy. We call the model the "twisted crystal model 20%" because we deal again with an HTI model whose axis of symmetry rotates with depth, and its anisotropy is 20%. The density-normalized elastic moduli are specified as follows:

$$\begin{pmatrix} 11.78 & 4.12 & 4.12 & 0 & 0 & 0 \\ & 16.42 & 5.28 & 0 & 0 & 0 \\ & & 16.42 & 0 & 0 & 0 \\ & & & 5.56 & 0 & 0 \\ & & & & 4.86 & 0 \\ & & & & & 4.86 \end{pmatrix}$$

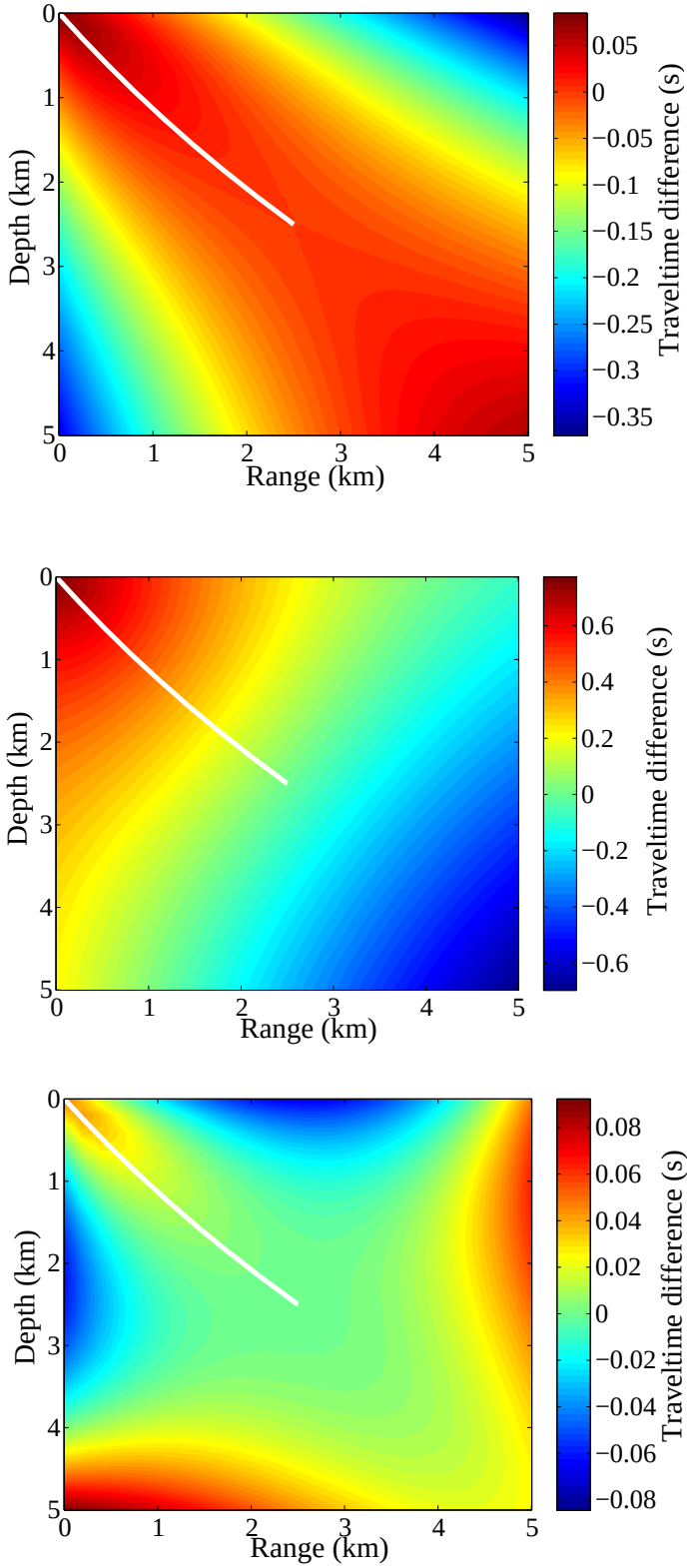

Figure 16: Traveltime differences $T(R',S) - T_{ex}(R',S)$ (in seconds) in the inhomogeneous "twisted crystal model 8%". $T_{ex}(R',S)$ - FORT traveltime. Top: $T(R',S) = T_{lin}(R',S)$ - quadratic terms suppressed; middle: $T(R',S) = T_{quad}(R',S)$ - linear terms suppressed; bottom: $T(R',S)$ - the complete two-point paraxial traveltime determined from formula 1. Points S and R are situated at the beginning and end of the reference ray - white curve. Point S is situated at (0,0). Point R is situated at (2.5,2.5) and points R' in the grid covering the studied region.

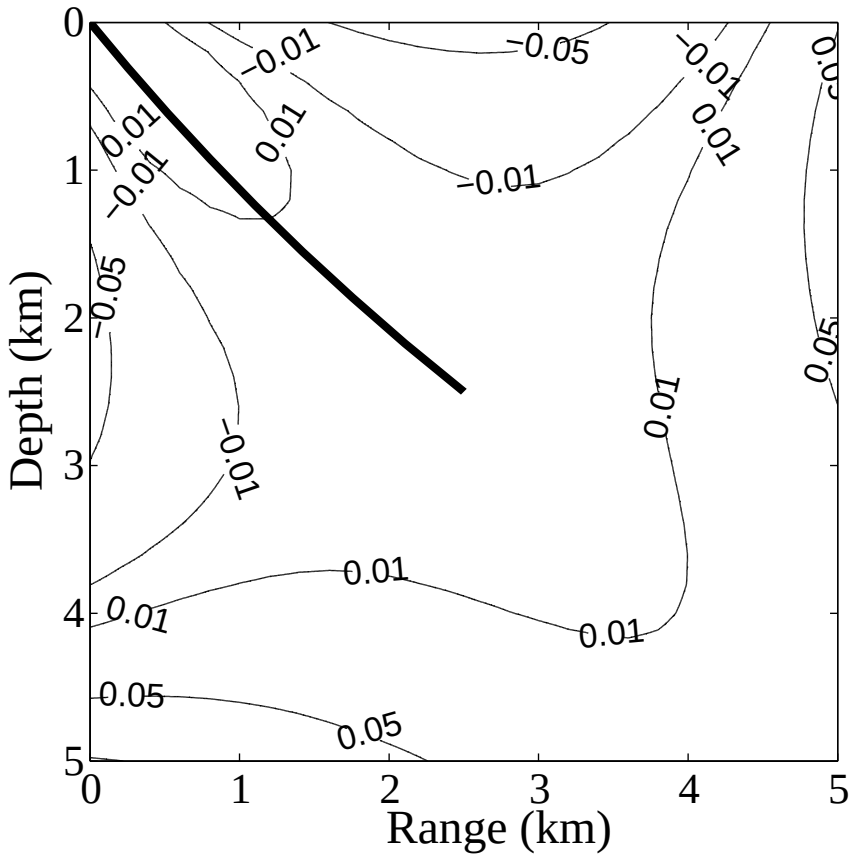

Figure 17: Traveltime differences $T(R', S) - T_{ex}(R', S)$ (in seconds) in the inhomogeneous "twisted crystal model 8%". $T_{ex}(R', S)$ - FORT traveltime. The plot corresponds to the bottom plot of Figure 16, where $T(R', S)$ is the complete two-point paraxial traveltime determined from formula 1. Points S and R are situated at the beginning and end of the reference ray - black curve. Point S is situated at (0,0). Point R is situated at (2.5,2.5) and points R' in the grid covering the studied region.

at $z = 0$ km and

$$\begin{pmatrix} 21.17926 & 6.38126 & 7.0675 & 0 & 0 & -1.769 \\ & 21.17926 & 7.0675 & 0 & 0 & -1.769 \\ & & 24.9155 & 0 & 0 & -0.8845 \\ & & & 7.93276 & -0.53376 & 0 \\ & & & & 7.93276 & 0 \\ & & & & & 7.59726 \end{pmatrix}$$

at $z = 5$ km. The Thomsen parameters (referenced to the axis of symmetry) are constant throughout: $\epsilon = 0.197$ and $\delta = 0.2$. The axis of symmetry makes an angle of 0^0 at $z = 0$ km and -45^0 at $z = 5$ km. The moduli between $z = 0$ and 5 km are again obtained by linear interpolation.

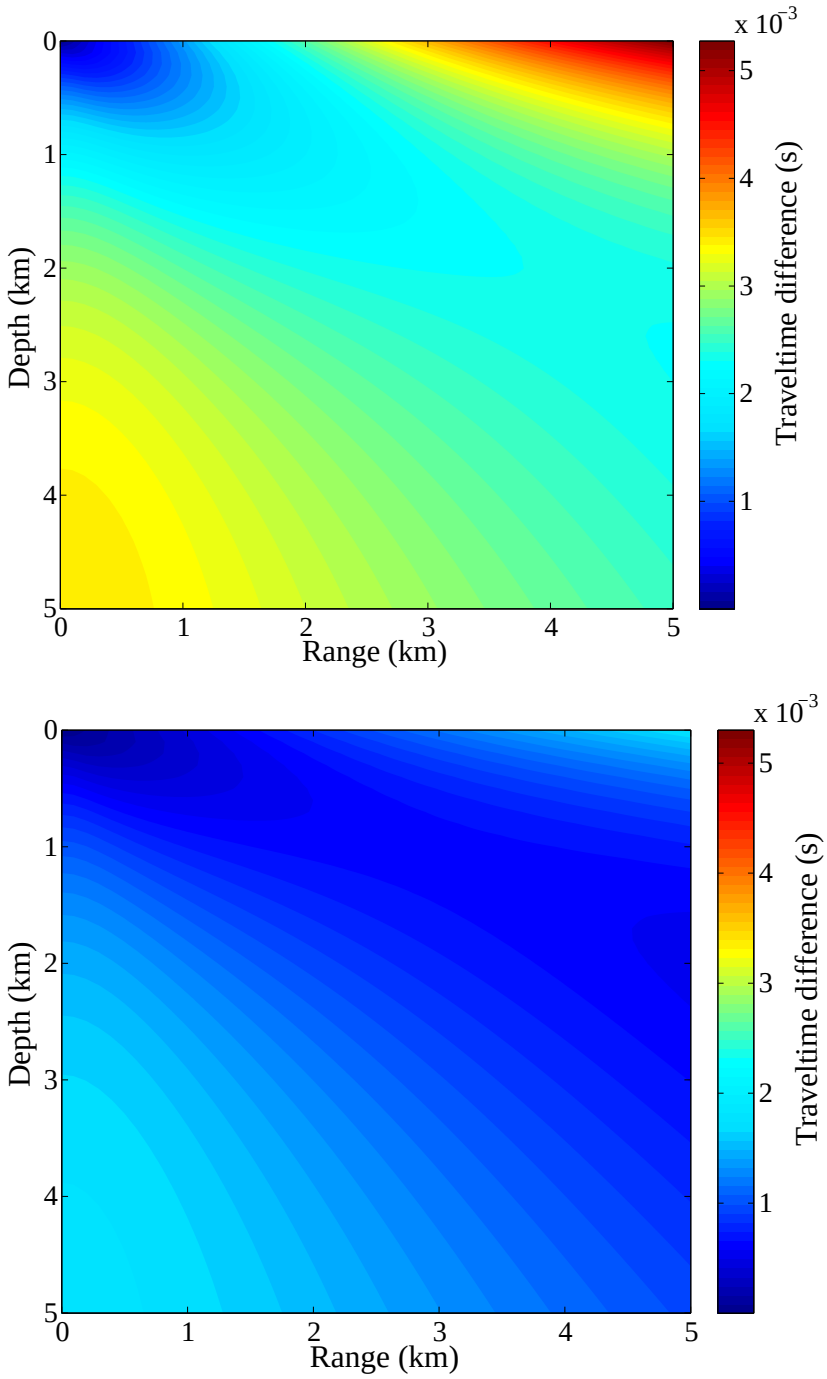

Figure 18: Application of the two-point paraxial traveltime formula to the estimation of traveltimes between shifted source S' and the system of receivers R'. The plots show the traveltime differences $|T(R', S') - T_{ex}(R', S')|$ (in seconds) in the inhomogeneous "twisted crystal model 8%". Shifted source S' at (0,0) and shifted receivers R' in the grid covering the studied region. Top: the source and receivers shifted vertically by 0.8 km. Bottom: the same as above after the Shanks transform.

The upper plot of Figure 19 shows the traveltime differences for the"twisted crystal model 20%" and the same configuration as in Figure 18. The bottom plot shows the differences after the Shanks transform. We can see that traveltime differences in both plots are smaller than in Figure 18. This is because of the smaller vertical gradient in the model used to generate the plots in Figure 19. Due to it, rays in Figure 19 are less curved than in Figure 18 and formula 1 works better. The more the reference ray is curved, the narrower the vicinity of the reference ray, in which formula 1 yields accurate results.

4 CONCLUSIONS

The above tests of the two-point paraxial traveltime formula 1 show its potential to estimate, approximately, two-point traveltimes in a rather broad vicinity of a single reference ray, along which quantities obtained during ray tracing and linear dynamic ray tracing between points S and R are available. Formula 1 is applicable to very general 3D smoothly laterally varying isotropic or anisotropic structures with or without smooth curved interfaces. Anisotropy of arbitrary type and strength may be considered. The positions of both points S and R may be varied arbitrarily. In the numerical tests, we concentrated on studying the two-point paraxial traveltimes of P-waves propagating in 2D inhomogeneous isotropic and anisotropic media. The tests were made for point S fixed and R varying as well as for both S and R varying.

Our tests demonstrated the crucial role of dynamic ray tracing in the two-point paraxial traveltime computations. While the linear part of formula 1 (with respect to the spatial coordinates) yields accurate estimates of the two-point traveltime only in the very close vicinity of the reference ray around point R, addition of the quadratic terms, whose coefficients are calculated from dynamic ray tracing, broadens the region of high accuracy of the estimated two-point traveltimes considerably. The accuracy increases not only in the region between S and R, but also beyond both points. The performed tests indicate that the accuracy of formula 1 in inhomogeneous media is primarily sensitive to the length and the curvature of the reference ray. The accuracy depends only weakly on anisotropy.

The tests performed have also shown that the accuracy of formula 9 for $T^2(R', S)$, which is exact in a homogeneous isotropic medium, decreases with increasing inhomogeneity of the medium to become comparably or even less accurate than formula 1 for $T(R', S)$. This observation, however, may be model-dependent and deserves further investigation.

As shown in numerical examples, the two-point paraxial traveltime formula can be used for very efficient estimation of the traveltime at an arbitrary point situated in a rather broad vicinity of the reference ray between points S and R. Since the ray tracing and dynamic ray tracing quantities are available at any point of the reference ray between S and R, we can, without any additional expenses, consider any such point as point R and apply formula 1 at its position.

The applicability of formula 1 also has some limitations. The formula is not expected to work properly in strongly varying media and in media, in which multipathing may

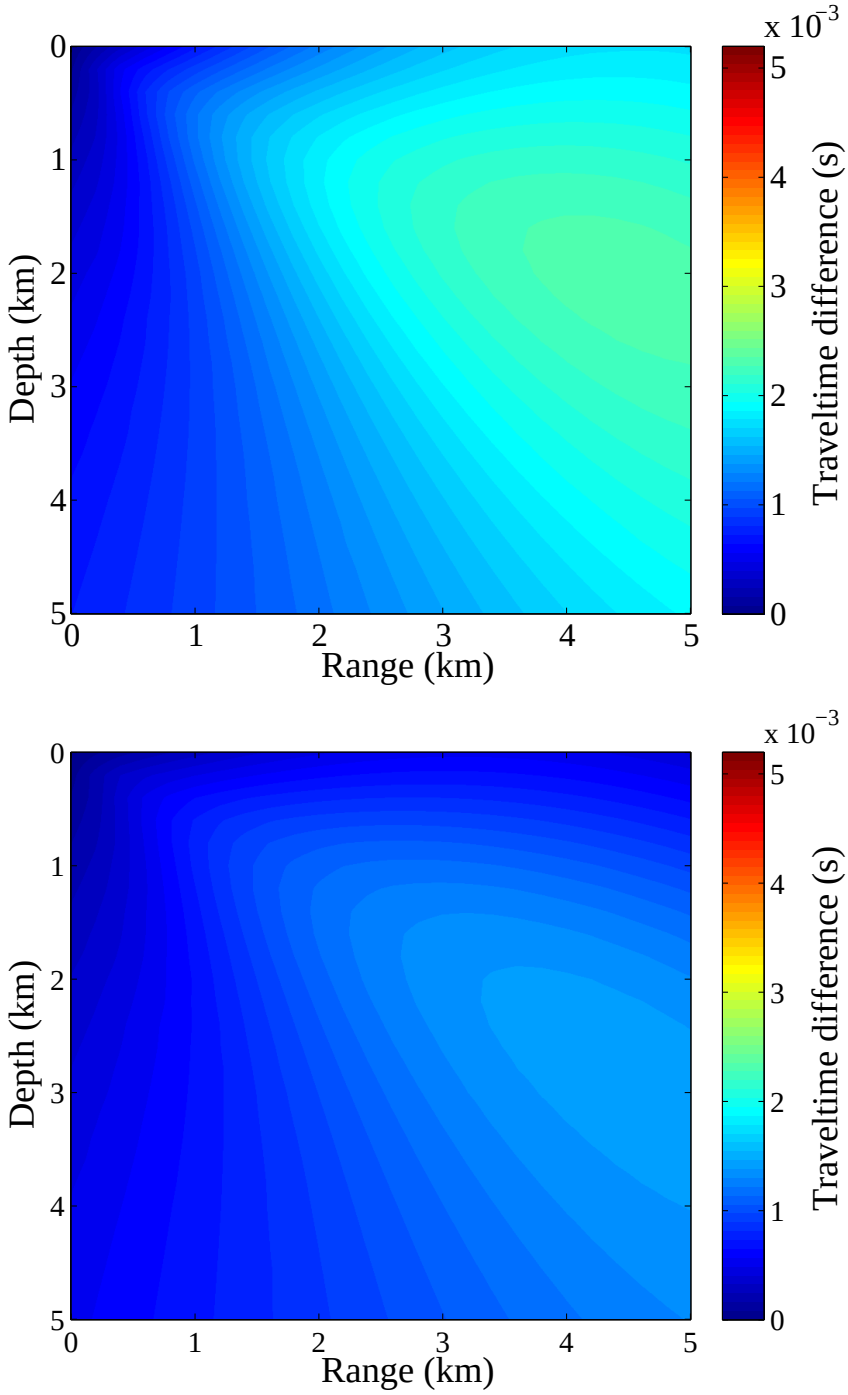

Figure 19: Application of the two-point paraxial traveltime formula to the estimation of traveltimes between shifted source S' and the system of receivers R'. The plots show the traveltime differences $|T(R', S') - T_{ex}(R', S')|$ (in seconds) in the inhomogeneous "twisted crystal model 20%". Shifted source S' at (0,0) and shifted receivers R' in the grid covering the studied region. Top: the source shifted vertically by 0.8 km and receivers horizontally by 0.4 km. Bottom: the same as above after the Shanks transform.

occur. Its accuracy decreases, as illustrated in this paper (see Figure 6), with decreasing time $T(R, S)$ between points S and R on the reference ray.

The properties of the two-point paraxial traveltime formula were mostly illustrated by numerical comparisons. Certain conclusions about the properties of the formula can also be deduced from its form and behavior in homogeneous media. We have shown that, in homogeneous isotropic or anisotropic media, formula 1 yields exact results along the reference ray, inside and outside interval specified by points S and R. In homogeneous or weakly inhomogeneous isotropic or anisotropic media, it yields highly accurate results in the direction perpendicular to the reference ray at R. This can be observed as cross-like regions of high accuracy in the vicinity of point R, see Figures 3, 15 and 17.

There are many possible applications of the two-point paraxial traveltime formula in seismology and seismic exploration. These applications include fast and flexible two-point traveltime calculations between sources and receivers, whose positions are specified in Cartesian coordinates and which are situated close to a known reference ray. A few possible applications were discussed by Červený et al. (2012). For example, they include typical situations in reflection surveys, in which source S and receiver R are situated on a measurement surface (the Earth's surface, ocean bottom). If we know the reference ray of a reflected wave from S to R and the corresponding traveltime $T(R, S)$, the proposed formula can be used to calculate traveltime $T(R', S')$ for any points S' and R' situated in a vicinity of S and R without ray tracing between S' and R'. This applies to common source, common offset, common midpoint, common reflection surface configuration, etc. The formula may also find useful applications in microseismic monitoring, location of microearthquakes, computation of Fresnel volumes and Fresnel zones, etc. In this paper, we have presented another application, which may play an important role in Kirchhoff modeling, migration or velocity estimation. Specifically, we presented the estimation of the two-point traveltimes $T(R', S')$ between the shifted source S' and the shifted system of receivers R'. If $T(R, S)$ and the ray-tracing and dynamic ray-tracing quantities calculated between S and R are known, it is an easy task, which can be repeated without additional ray tracing and dynamic ray tracing as many times as necessary. Comparison with results of the numerical solution of the eikonal-based partial differential equation indicates that the two-point paraxial traveltime formula may provide results of higher accuracy. As shown in Figures 11, 12 and 18, 19 the shifts of points S and R may be quite large in comparison with their distance. Points S and R may be shifted, without any problem, in different ways; the medium may be 3D inhomogeneous isotropic or anisotropic, with or without smooth curved interfaces. In this paper, we have concentrated on media without interfaces. Preliminary tests in media with interfaces indicate again the high accuracy of formula 1.

Many published papers have been devoted to the theory of the two-point paraxial traveltimes, for more details refer to the Introduction, but only a few of them also to the study of their accuracy. The most extensive tests were performed by Gjøystdal et al. (1984). Their approach is, however, applicable only to isotropic media and uses the *non-linear* DRT based on the Ricatti equation. The approach tested in this paper is applicable both to isotropic and *anisotropic* media and uses the *linear* DRT, which allows the use of the ray propagator matrix concept. This makes it much easier to compute the

quadratic terms of the two-point traveltime formula, as compared to using DRT based on the Riccatti equation.

ACKNOWLEDGEMENTS

We would like to express our gratitude to Joachim Mispel, three anonymous referees and the Associate Editor, Claudia Vanelle, for their stimulating comments. We are grateful to Seismic Wave Analysis Group (SWAG) of KAUST, Saudi Arabia, project "Seismic waves in complex 3-D structures" (SW3D), to Research Projects 210/11/0117 and 210/10/0736 of the Grant Agency of the Czech Republic and to Research Project MSM0021620860 of the Ministry of Education of the Czech Republic for support. E. Iversen acknowledges support from the Research Council of Norway and from the European Community's FP7 Consortium Project AIM "Advanced Industrial Microseismic Monitoring", Grant Agreement No. 230669. This paper will appear in the September-October 2013 issue of Geophysics devoted to the proceedings of 15th International Workshop on Seismic Anisotropy.

REFERENCES

Alkhalifah, T., and S. Fomel, 2010. An eikonal-based formulation for traveltime perturbation with respect to the source location: Geophysics, **75**, No. 6, T175–T183.

Bender, C. M., and S. A. Orszag, 1978. Advanced mathematical methods for scientists and engineers: McGraw-Hill, Singapore.

Bortfeld, R. 1989. Geometrical ray theory: Rays and traveltimes in seismic systems (second-order approximation of traveltimes): Geophysics **54**, 342–349.

Červený, V., 2001. Seismic ray theory: Cambridge Univ. Press, Cambridge.

Červený, V., E. Iversen, and I. Pšenčík, 2012. Two-point paraxial travel times in an inhomogeneous anisotropic medium: Geophysical Journal International, **189**, 1597-1610.

Červený, V., L. Klimeš and I. Pšenčík, 1984. Paraxial ray approximations in the computation of seismic wavefields in inhomogeneous media: Geophys. J. R. astr. Soc., **79**, 89–104.

Červený, V., and T.J. Moser, 2007. Ray propagator matrices in three-dimensional anisotropic inhomogeneous layered structures: Geophys. J. Int., **168**, 593–604.

Gjøystdal, H., I. E. Reinhardsen, and B. Ursin, 1984. Traveltime and wavefront curvature calculations in three-dimensional inhomogeneous layered media with curved interfaces: Geophysics, **49**, 1466–1494.

Hamilton, W.R., 1837. Third supplement to an essay on the theory of systems of rays: Transactions of Royal Irish Academy, **17**, 1–144.

Hubral, P., J. Schleicher, M. Tygel, 1992. Three-dimensional paraxial ray properties, Part 1: Basic relations: J. Seismic Exploration, **1**, 265–279.

Klimeš, L., 2009. Relation between the propagator matrix of geodesic deviation and second-order derivation of characteristic function: Seismic Waves in Complex 3-D Structures, Report 19, pp. 103–114, Charles Univ., Faculty of Mathematics and Physics, Dept. of Geophysics, Prague (Online at: http: //sw3d.cz).

Luneburg, R.K., 1964. Mathematical Theory of Optics: University of California Press, Berkeley.

Mispel, J., E. Iversen, V. Vinje, R. Laurain and I. Lecomte, 2003. Local Two-Way Traveltime Approximations in 3-D Media: 65th Annual Meeting, EAGE, Extended Abstracts, P046.

Moser, T.J., and V. Červený, 2007. Paraxial ray methods for anisotropic inhomogeneous media: Geophysical Prospecting, **55**, 21–37.

Pšenčík, I., and V. Farra, 2005. First-order ray tracing for qP waves in inhomogeneous weakly anisotropic media: Geophysics, **70**, No. 6, D65–D75.

Pšenčík, I., and V. Farra, 2007. First-order P-wave ray synthetic seismograms in inhomogeneous weakly anisotropic media: Geophysical Journal International, **170**, 1243–1252.

Schleicher J., M.Tygel, and P. Hubral, 1993. Parabolic and hyperbolic paraxial two-point traveltimes in 3D media: Geophysical Prospecting **41**, 495–513.

Ursin, B., 1982. Quadratic wavefront and travel time approximations in inhomogeneous layered media with curved interfaces: Geophysics, **47**, 1012–1021.

Vanelle, C., and D. Gajewski, 2002. Second-order interpolation of traveltimes: Geophysical Prospecting, **50**, 73–83.

Vanelle, C., and D. Gajewski, 2003. Determination of geometrical spreading from traveltimes: Journal of Applied Geophysics, **54**, 391–400.

APPENDIX A
TWO-POINT PARAXIAL TRAVELTIME $T(R', S')$ IN A HOMOGENEOUS MEDIUM

Formula 1 for the two-point paraxial traveltime $T(R', S')$ simplifies considerably in homogeneous anisotropic or isotropic media. Rays in homogeneous media are straight lines, therefore, numerical ray tracing is not necessary. In this case, the 4×4 ray propagator matrix $\mathbf{\Pi}(R, S)$ can be determined analytically so that neither the dynamic ray tracing is required. Moreover, only one of the four 2×2 submatrices of $\mathbf{\Pi}(R, S)$ is non-zero, specifically $\mathbf{Q}_2(R, S)$.

Exact expressions for $T(R', S')$ in homogeneous media can be determined from simple geometrical considerations. This offers a simple way of estimating the accuracy of the approximate formula 1 in this special case. In addition, these exact expressions are useful tools for the correct understanding of phenomena present in the figures of this paper.

In a *homogeneous anisotropic medium*, the two-point paraxial traveltime formula 1 reduces to

$$T(R', S') = T(R, S) + p_i(\delta x_i^R - \delta x_i^S) + \frac{1}{2} f_{Mi} (\mathbf{Q}_2^{-1})_{MN} f_{Nj} (\delta x_i^R - \delta x_i^S)(\delta x_j^R - \delta x_j^S). \quad (A-1)$$

Here we have used the same notation as in formula 1. Since slowness vector $\mathbf{p}$ and vectors $\mathbf{f}_M$ are constant along the reference ray, i.e. they are the same at points S and R, we do not use arguments and superscripts S and R for them.

Let us consider points S′ and R′ situated on the reference ray, i.e. let us consider *vectors $\delta\mathbf{x}^S$ and $\delta\mathbf{x}^R$ parallel to the reference ray.* Since vectors $\mathbf{f}_M$ are perpendicular to the reference ray, the quadratic term vanishes and equation A-1 reduces to:

$$T(R', S') = T(R, S) + p_i[x_i(R') - x_i(S')] - p_i[x_i(R) - x_i(S)]. \quad (A-2)$$

If we take into account the obvious relation $T(R, S) = (\partial\tau/\partial x_i)[x_i(R) - x_i(S)] = p_i[x_i(R) - x_i(S)]$ (remember: in anisotropic media, slowness vector $\mathbf{p}$ need not be parallel to vector $\mathbf{x}(R) - \mathbf{x}(S)$), we have

$$p_i[x_i(R') - x_i(S')] = T_{exact}(R', S') \ , \qquad p_i[x_i(R) - x_i(S)] = T_{exact}(R, S) = T(R, S) \ . \quad (A-3)$$

Symbol $T_{exact}(R', S')$ in equation A-3 denotes the exact traveltime between the points specified in the argument. Inserting equation A-3 in equation A-2 yields

$$T(R', S') = T(R, S) + T_{exact}(R', S') - T(R, S) = T_{exact}(R', S') \ . \quad (A-4)$$

We can see that the two-point paraxial traveltime formula 1 yields exact results along reference rays in homogeneous isotropic or anisotropic media also for points situated inside and outside the interval $\overline{SR}$. It should be emphasized that the two-point paraxial traveltime formula 1 is exact along a ray only in a homogeneous medium (when the ray is a straight line). In inhomogeneous media, formula 1 is always only approximate.

Another situation, in which formula 1 yields exact results is for $\delta\mathbf{x}^S = \delta\mathbf{x}^R$ in homogeneous isotropic or anisotropic media. This follows immediately from equation A-1 and it

is simply understandable since this case represents a parallel shift of the whole reference ray between points S and R into the new position between S′ and R′.

Formula A-1 further simplifies in *homogeneous isotropic media.* In this case, the expression for $\mathbf{Q}_2(R,S)$ simplifies considerably:

$$[\mathbf{Q}_2(R,S)]_{MN} = V^2 T(R,S)\delta_{MN} \ , \qquad (A-5)$$

see Červený (2001, equation 4.8.3). In equation A-5, V denotes the P- or S-wave velocity in a homogeneous isotropic medium. Inserting equation A-5 into equation A-1 yields

$$T(R',S') = T(R,S) + p_i(\delta x_i^R - \delta x_i^S) + \frac{1}{2V^2T(R,S)}(\delta_{ij} - v^2 p_i p_j)(\delta x_i^R - \delta x_i^S)(\delta x_j^R - \delta x_j^S) \ . \qquad (A-6)$$

Here we have used the fact that vectors $\mathbf{f}_M$ are unit and mutually orthogonal in isotropic media, and the relation $f_{Mi}f_{Nj} = \delta_{ij} - V^2 p_i p_j$. For *vectors* $\delta\mathbf{x}^S$ *and* $\delta\mathbf{x}^R$ *perpendicular to the reference ray*, i.e. for $p_i(\delta x_i^R - \delta x_i^S) = 0$, equation A-6 reduces to:

$$T(R',S') = T(R,S) + \frac{1}{2V^2T(R,S)}(\delta x_i^R - \delta x_i^S)(\delta x_i^R - \delta x_i^S) \ . \qquad (A-7)$$

This is an approximate, but highly accurate equation. This can be proved by comparing it with the exact expression $T_{exact}(R',S')$, which can be obtained from simple geometric considerations. The exact expression reads:

$$T_{exact}(R',S') = [T^2(R,S) + V^{-2}(\delta x_i^R - \delta x_i^S)(\delta x_i^R - \delta x_i^S)]^{1/2} \ . \qquad (A-8)$$

For small $V^{-2}T^{-2}(R,S)(\delta x_i^R - \delta x_i^S)(\delta x_i^R - \delta x_i^S)$, we can expand equation A-8 into a Taylor series whose leading terms are:

$$T_{exact}(R',S') = T(R,S) + \frac{1}{2V^2T(R,S)}(\delta x_i^R - \delta x_i^S)(\delta x_i^R - \delta x_i^S) + \ldots \ . \qquad (A-9)$$

Thus, the approximate expression A-7 coincides with the expansion of the exact expression A-8 to the quadratic terms in $\delta x_i^R - \delta x_i^S$. Since the next non-zero term in the Taylor expansion of expression A-8 is of the order $(\delta x_i^R - \delta x_i^S)^4$, the error of the approximate expression A-7 is of this order. Since this term is negative, equation A-7 yields approximate traveltimes, which are always larger than exact ones. Expression A-7 approximates expression A-8 well if the term $V^{-2}T^{-2}(R,S)(\delta x_i^R - \delta x_i^S)(\delta x_i^R - \delta x_i^S)$ is small. This condition explains unsatisfactory performance of formula 1 for $T(R,S) \to 0$, see, for example, the upper left plot in Figure 6.

For completeness, let us also describe the properties of the expression for the *square of the two-point paraxial traveltime for a homogeneous isotropic medium*, $T^2(R',S')$. If we neglect terms of order higher than two in $(\delta\mathbf{x}^R - \delta\mathbf{x}^S)$ in the squared expression A-6, we get

$$T^2(R',S') = T^2(R,S) + 2T(R,S)p_i(\delta x_i^R - \delta x_i^S) + V^{-2}(\delta x_i^R - \delta x_i^S)(\delta x_i^R - \delta x_i^S) \ . \qquad (A-10)$$

The exact formula reads:

$$T^2_{exact}(R',S') = V^{-2}[x_i(R') - x_i(S')][x_i(R') - x_i(S')] \ . \qquad (A-11)$$

If we take into account that

$$x_i(R') - x_i(S') = \delta x_i^R + x_i(R) - x_i(S) - \delta x_i^S \ , \qquad (A-12)$$

A-11 can be altered to read

$$T^2_{exact}(R', S') = T^2(R, S) + 2T(R, S)p_i(\delta x_i^R - \delta x_i^S) + V^{-2}(\delta x_i^R - \delta x_i^S)(\delta x_i^R - \delta x_i^S) \ . \quad (A-13)$$

Equations A-10 and A-13 are identical, which implies that equation A-10 is exact. We can also see that the problems with the accuracy of the two-point paraxial traveltime formula for $T(R, S) \to 0$, observed in equation A-7, disappeared in the expression for $T^2(R', S')$. See also Ursin (1982), Gjøystdal et al. (1984), Schleicher et al. (1993), who proved it for equations of different form from ours.

APPENDIX B
SHANKS TRANSFORM

The Shanks transform is a useful way of improving the convergence rate of a series. Let us consider a Taylor series expansion of function $T(x)$:

$$T(x) = C_0 + C_1 x + C_2 x^2 + \cdots \ . \qquad (B-1)$$

Here C_0, C_1 and C_2 are coefficients of the expansion. We can isolate and remove the most transient behavior of expansion B-1 by first defining the following parameters:

$$A_0 = C_0 \ , \quad A_1 = C_0 + C_1 x \ , \quad A_2 = C_0 + C_1 x + C_2 x^2 \qquad (B-2)$$

The Shanks transform representation (Bender and Orszag, 1978) of B-1 is then given by:

$$T(x) \approx \frac{A_0 A_2 - A_1^2}{A_0 - 2A_1 + A_2} \qquad (B-3)$$

This transformation creates a new series which often converges more rapidly than the old series B-1.

Numerical computations using the Shanks transform must be dealt with caution as computer processors are limited in precision to the numbers they can resolve. Thus, when x is extremely small, the denominator $A_0 - 2A_1 + A_2$ of B-3 is dominated by this round-off error and its accuracy is likely to be lower than the original series B-1.